

Permutation p -value approximation via generalized Stolarsky invariance

Hera Yu He, Kinjal Basu, Qingyuan Zhao, Art B. Owen

Department of Statistics

Sequoia Hall

Stanford University

Stanford, CA 94305

e-mail: [\(hera, kinjal, qyzhao, owen\)@stanford.edu](mailto:(hera, kinjal, qyzhao, owen)@stanford.edu)

Abstract: When it is necessary to approximate a small permutation p -value p , then simulation is very costly. For linear statistics, a Gaussian approximation \hat{p}_1 reduces to the volume of a spherical cap. Using Stolarsky's (1973) invariance principle from discrepancy theory, we get a formula for the mean of $(\hat{p}_1 - p)^2$ over all spherical caps. From a theorem of Brauchart and Dick (2013) we get such a formula averaging only over spherical caps of volume exactly \hat{p}_1 . We also derive an improved estimator \hat{p}_2 equal to the average true p -value over spherical caps of size \hat{p}_1 containing the original data point x_0 on their boundary. This prevents \hat{p}_2 from going below $1/N$ when there are N unique permutations. We get a formula for the mean of $(\hat{p}_2 - p)^2$ and find numerically that the root mean squared error of \hat{p}_2 is roughly proportional to \hat{p}_2 and much smaller than that of \hat{p}_1 .

1. Introduction

Permutation methods are commonly used to obtain p -values in genomic applications. The exact permutation p -value is typically too expensive to compute and one instead samples $M - 1$ random permutations and reports an approximate p -value as the number of suitably extreme outcomes divided by M . The original data are counted in both numerator and denominator, and the p -value will not be smaller than $1/M$.

Small p -values are often required in settings where a great many tests are conducted. When a very small p -value ϵ is required, then for reasonable power, M must be at least a modest multiple of $1/\epsilon$. For instance in genome wide association studies (GWAS) the customary threshold for significance is $\epsilon = 5 \times 10^{-8}$, making permutation methods prohibitively expensive for such problems. Advances in multiple testing, such as the false discovery rate of [Benjamini and Hochberg \(1995\)](#), mitigate but do not remove the need to establish small p -values.

For linear test statistics, as we show below, the permutation p -value is the fraction of permuted data vectors lying in a given spherical cap subset of a d -dimensional sphere $\mathbb{S}^d = \{z \in \mathbb{R}^{d+1} \mid z^T z = 1\}$. A natural but crude approximation to that p -value is the fraction \hat{p} of the sphere's surface volume contained in that spherical cap.

Stolarsky's invariance principal gives a remarkable description of the accuracy of this approximation \hat{p} . For $\mathbf{y} \in \mathbb{S}^d$ and $t \in [-1, 1]$ we can define the spherical cap of center \mathbf{y} and height t via $C(\mathbf{y}; t) = \{\mathbf{z} \in \mathbb{S}^d \mid \langle \mathbf{y}, \mathbf{z} \rangle \geq t\}$. For $\mathbf{x}_0, \dots, \mathbf{x}_{N-1} \in \mathbb{S}^d$, let $p(\mathbf{y}, t)$ be the fraction of those N points that lie in $C(\mathbf{y}; t)$ and let $\hat{p}(\mathbf{y}, t) = \hat{p}(t) = \text{vol}(C(\mathbf{y}; t))/\text{vol}(\mathbb{S}^d)$. The squared L_2 spherical cap discrepancy of these points is

$$L_2(\mathbf{x}_0, \dots, \mathbf{x}_{N-1})^2 = \int_{-1}^1 \int_{S_d} |\hat{p}(t) - p(\mathbf{z}, t)|^2 d\sigma_d(\mathbf{z}) dt.$$

Stolarsky (1973) shows that

$$\frac{d\omega_d}{\omega_{d+1}} \times L_2(\cdot)^2 = \int_{\mathbb{S}^d} \int_{\mathbb{S}^d} \|\mathbf{x} - \mathbf{y}\| d\sigma_d(\mathbf{x}) d\sigma_d(\mathbf{y}) - \frac{1}{N^2} \sum_{k,l=0}^{N-1} \|\mathbf{x}_k - \mathbf{x}_l\| \quad (1.1)$$

where σ_d is the uniform (Haar) measure on \mathbb{S}^d and ω_d is the (surface) volume of \mathbb{S}^d . Equation (1.1) relates the mean squared error of \hat{p} to the mean absolute Euclidean distance among the N points. In our applications, the N points will be the distinct permuted values of a data vector, but the formula holds for an arbitrary set of N points.

The left side of (1.1) is, up to normalization, a mean squared discrepancy over spherical caps. This average of $(\hat{p} - p)^2$ includes p -values of all sizes between 0 and 1. It is not then a very good accuracy measure when \hat{p} turns out to be very small. It would be more useful to get such a mean squared error taken over caps of exactly the size \hat{p} , and no others.

Brauchart and Dick (2013) consider quasi-Monte Carlo (QMC) sampling in the sphere. They generalize Stolarsky's discrepancy formula to include a weighting function on the height t . By specializing their formula, we get an expression for the mean of $(\hat{p} - p)^2$ over spherical caps of any fixed size.

Discrepancy theory plays a prominent role in QMC (Niederreiter, 1992), which is about approximating an integral by a sample average. The present setting is in a sense the reverse of QMC: the discrete average over permutations is the exact value, and the integral over a continuum is the approximation. A second difference is that the QMC literature focusses on choosing N points to minimize a criterion such as (1.1), whereas here the N points are determined by the problem.

We present several results for the mean of $(\hat{p} - p)^2$ under different conditions. In addition to fixing the size of the caps we can restrict the mean squared error to only be over caps centered on points \mathbf{y} satisfying $\langle \mathbf{y}, \mathbf{x}_0 \rangle = \langle \mathbf{y}_0, \mathbf{x}_0 \rangle$ where \mathbf{x}_0 is the original (unpermuted) \mathbf{x} vector and \mathbf{y}_0 is the observed \mathbf{y} value. We can obtain this result by further extending Brauchart and Dick's generalization of Stolarsky's invariance. We call this the 'finer approximation' and will show it has advantages over constraining only the height of the caps. More generally, the point \mathbf{x}_c could be any of the permuted \mathbf{x} vectors, such as the one that happens to be closest to \mathbf{y}_0 .

Although we found these results via invariance we can also obtain them via probabilistic arguments. As a consequence we have a probabilistic derivation

of Stolarsky's formula. Some of our results are for arbitrary \mathbf{x} , but our best computational formulas are for the case where the variable \mathbf{x} is binary, as it would be in experiments comparing treatment and control groups.

The rest of the paper is organized as follows. Section 2 presents some context on permutation tests and gives some results from spherical geometry. In Section 3 we use Stolarsky's invariance principle as generalized by [Brauchart and Dick \(2013\)](#) to obtain the mean squared error between the true p -value and its continuous approximation \hat{p}_1 , taken over all spherical caps of volume \hat{p}_1 . This section also has a probabilistic derivation of that mean squared error. In Section 4 we describe some finer approximations \tilde{p} for the p -value. These condition on not just the volume of the spherical cap but also on its distance from the original data point \mathbf{x}_0 , or from some other point, such as the closest permutation of \mathbf{x}_0 to \mathbf{y}_0 . By always including the original point we ensure that $\tilde{p} \geq 1/N$. That is a desirable property because the true permutation p -value cannot be smaller than $1/N$. In Section 5 we modify the proof in [Brauchart and Dick \(2013\)](#), to further generalize their invariance results to include the mean squared error of the finer approximations. Section 6 extends our estimates to two-sided testing. Section 7 illustrates our p -value approximations numerically. We see that an RMS error in the finer approximate p -values is of the same order of magnitude as those p -values themselves. Section 8 makes a numerical comparison to saddlepoint methods. Section 9 discusses the results and gives more details about the bioinformatics problems that motivate the search for approximations to the permutation distribution. Most of the proofs are in the Appendix, Section 10.

2. Background and notation

The raw data contain points (X_i, Y_i) for $i = 1, \dots, n$. The sample correlation of these points is $\hat{\rho} = \mathbf{x}_0^\top \mathbf{y}_0$ where \mathbf{x}_0 has components $(X_i - \bar{X})/s_X$ for $\bar{X} = (1/n) \sum_{i=1}^n X_i$, $s_X^2 = (1/n) \sum_{i=1}^n (X_i - \bar{X})^2$ and \bar{Y} and s_Y are defined similarly. We assume that s_X and s_Y are positive. Both \mathbf{x}_0 and \mathbf{y}_0 belong to \mathbb{S}^{n-1} . Moreover they belong to $\{\mathbf{z} \in \mathbb{S}^{n-1} \mid \mathbf{z}^\top \mathbf{1}_n = 0\}$. We can use an orthogonal matrix to rotate the points of this set onto $\mathbb{S}^{n-2} \times \{0\}$. As a result, we may simply work with $\mathbf{x}_0, \mathbf{y}_0 \in \mathbb{S}^d$ where $d = n - 2$.

The quantity $\hat{\rho}$ measures association between X and Y . It can be used as such a measure if the X_i are fixed and Y_i observed conditionally, or vice versa, or if the (X_i, Y_i) pairs are independently sampled from some joint distribution. Let π be a permutation of the indices $1, \dots, n$. There are $n!$ vectors \mathbf{x}_π that result from centering and scaling $X_\pi = (X_{\pi(1)}, X_{\pi(2)}, \dots, X_{\pi(n)})$. The permutation p -value is $p = (1/n!) \sum_\pi \mathbf{1}(\mathbf{x}_\pi^\top \mathbf{y}_0 \geq \mathbf{x}_0^\top \mathbf{y}_0)$. The justification for this p -value relies on the group structure of permutations ([Lehmann and Romano, 2005](#)). For a cautionary tale on the use of permutation sets without a group structure, see [Southworth et al. \(2009\)](#). For notational simplicity we assume $\hat{\rho} > 0$ and work with one-sided p -values. Negative $\hat{\rho}$ can be handled similarly, or simply by switching the group labels. For two-sided p -values see Section 6.

Our proposals are computationally most attractive in the case where X_i takes

on just two values, such as 0 and 1. Then $\hat{\rho}$ is a two-sample test statistic. If there are m_0 observations with $X_i = 0$ and m_1 with $X_i = 1$ then \mathbf{x}_0 contains m_0 components equal to $-\sqrt{m_1/(nm_0)}$ and m_1 components equal to $+\sqrt{m_0/(nm_1)}$. Some formulas involve the smaller sample size, $\underline{m} \equiv \min(m_0, m_1)$.

For this two-sample case there are only $N = \binom{m_0+m_1}{m_0}$ distinct permutations of \mathbf{x}_0 . Calling these $\mathbf{x}_0, \mathbf{x}_1, \dots, \mathbf{x}_{N-1}$ we find that

$$p = \frac{1}{N} \sum_{k=0}^{N-1} \mathbf{1}(\mathbf{x}_k^\top \mathbf{y}_0 \geq \hat{\rho}). \quad (2.1)$$

Now suppose that there are exactly r indices for which \mathbf{x}_k is positive and \mathbf{x}_l is negative. There are then r indices with the reverse pattern too. We say that \mathbf{x}_k and \mathbf{x}_l are at ‘swap distance r ’. In that case we easily find that

$$u(r) \equiv \mathbf{x}_k^\top \mathbf{x}_l = 1 - r \left(\frac{1}{m_0} + \frac{1}{m_1} \right). \quad (2.2)$$

We need some geometric properties of the unit sphere and spherical caps. The surface volume of \mathbb{S}^d is $\omega_d = 2\pi^{(d+1)/2}/\Gamma((d+1)/2)$. We use σ_d for the volume element in \mathbb{S}^d normalized so that $\sigma_d(\mathbb{S}^d) = 1$. The spherical cap $C(\mathbf{y}; t) = \{\mathbf{z} \in \mathbb{S}^d \mid \mathbf{z}^\top \mathbf{y} \geq t\}$ has volume

$$\sigma_d(C(\mathbf{y}; t)) = \begin{cases} \frac{1}{2} I_{1-t^2} \left(\frac{d}{2}, \frac{1}{2} \right), & 0 \leq t \leq 1 \\ 1 - \frac{1}{2} I_{1-t^2} \left(\frac{d}{2}, \frac{1}{2} \right), & -1 \leq t < 0 \end{cases}$$

where $I_t(a, b)$ is the incomplete beta function

$$I_t(a, b) = \frac{1}{B(a, b)} \int_0^t x^{a-1} (1-x)^{b-1} dx$$

with $B(a, b) = \int_0^1 x^{a-1} (1-x)^{b-1} dx$. Obviously, this volume is 0 if $t < -1$ and it is 1 if $t > 1$. This volume is independent of \mathbf{y} so we may write $\sigma_d(C(\cdot, t))$ for the volume. By symmetry, $\mathbf{1}(\mathbf{x} \in C(\mathbf{y}, t)) = \mathbf{1}(\mathbf{y} \in C(\mathbf{x}, t))$.

Our first approximation of the p -value is

$$\hat{p}_1(\hat{\rho}) = \sigma_d(C(\mathbf{y}; \hat{\rho})). \quad (2.3)$$

This approximation has two intuitive explanations. First, the true p -value is the proportion of permutations of \mathbf{x}_0 that lie in $C(\mathbf{y}_0; \hat{\rho})$, and $\sigma_d(C(\mathbf{y}_0; \hat{\rho}))$ is the proportion of the volume of \mathbb{S}^d in that set. Second, as we show in Proposition 2, $\hat{p}_1 = \mathbb{E}(p \mid \langle \mathbf{x}_0, \mathbf{y} \rangle = \hat{\rho})$ for $\mathbf{y} \sim \mathbf{U}(\mathbb{S}^d)$ as \mathbf{y}_0 would if the original Y_i were IID Gaussian. In Theorem 4, we find $\text{Var}(\hat{p}_1)$ under this assumption.

We frequently need to project $\mathbf{y} \in \mathbb{S}^d$ onto a point $\mathbf{x} \in \mathbb{S}^d$. In this representation $\mathbf{y} = t\mathbf{x} + \sqrt{1-t^2}\mathbf{y}^*$ where $t = \mathbf{y}^\top \mathbf{x} \in [-1, 1]$ and $\mathbf{y}^* \in \{\mathbf{z} \in \mathbb{S}^d \mid \mathbf{z}^\top \mathbf{x} = 0\}$ which is isomorphic to \mathbb{S}^{d-1} . The coordinates t and \mathbf{y}^* are unique. From equation (A.1) in Brauchart and Dick (2013) we get

$$d\sigma_d(\mathbf{y}) = \frac{\omega_{d-1}}{\omega_d} (1-t^2)^{d/2-1} dt d\sigma_{d-1}(\mathbf{y}^*). \quad (2.4)$$

In their case \mathbf{x} was $(0, 0, \dots, 1)$.

The intersection of two spherical caps of common height t is

$$C_2(\mathbf{x}, \mathbf{y}; t) \equiv C(\mathbf{x}; t) \cap C(\mathbf{y}; t).$$

We will need the volume of this intersection. [Lee and Kim \(2014\)](#) give a general solution for spherical cap intersections without requiring equal heights. They enumerate 25 cases, but our case does not correspond to any single such case and so we obtain the formula we need directly, below. We suspect it must be known already, but we were unable to find it in the literature.

Lemma 1. *Let $\mathbf{x}, \mathbf{y} \in \mathbb{S}^d$ and $-1 \leq t \leq 1$ and put $u = \mathbf{x}^\top \mathbf{y}$. Let $V_2(u; t, d) = \sigma_d(C_2(\mathbf{x}, \mathbf{y}; t))$. If $u = 1$, then $V_2(u; t, d) = \sigma_d(C(\mathbf{x}; t))$. If $-1 < u < 1$, then*

$$V_2(u; t, d) = \frac{\omega_{d-1}}{\omega_d} \int_t^1 (1 - s^2)^{\frac{d}{2}-1} \sigma_{d-1}(C(\mathbf{y}^*; \rho(s))) ds, \quad (2.5)$$

where $\rho(s) = (t - su)/\sqrt{(1 - s^2)(1 - u^2)}$. Finally, for $u = -1$,

$$V_2(u; t, d) = \begin{cases} 0, & t \geq 0 \\ \frac{\omega_{d-1}}{\omega_d} \int_{-|t|}^{|t|} (1 - s^2)^{\frac{d}{2}-1} ds, & \text{else.} \end{cases} \quad (2.6)$$

Proof. Let $\mathbf{z} \sim \mathbf{U}(\mathbb{S}^d)$. Then $V_2(u; t, d) = \sigma_d(C_2(\mathbf{x}, \mathbf{y}; t)) = \Pr(\mathbf{z} \in C_2(\mathbf{x}, \mathbf{y}; t))$. If $u = 1$ then $\mathbf{x} = \mathbf{y}$ and so $C_2(\mathbf{x}, \mathbf{y}; t) = C(\mathbf{x}; t)$. For $u < 1$, we project \mathbf{y} and \mathbf{z} onto \mathbf{x} , via $\mathbf{z} = s\mathbf{x} + \sqrt{1 - s^2}\mathbf{z}^*$ and $\mathbf{y} = u\mathbf{x} + \sqrt{1 - u^2}\mathbf{y}^*$. Now

$$\begin{aligned} V_2(u; t, d) &= \int_{\mathbb{S}^d} \mathbf{1}(\langle \mathbf{x}, \mathbf{z} \rangle \geq t) \mathbf{1}(\langle \mathbf{y}, \mathbf{z} \rangle \geq t) d\sigma(\mathbf{z}) \\ &= \int_{-1}^1 \mathbf{1}(s \geq t) \frac{\omega_{d-1}}{\omega_d} (1 - s^2)^{\frac{d}{2}-1} \\ &\quad \times \int_{\mathbb{S}^{d-1}} \mathbf{1}(su + \sqrt{1 - s^2}\sqrt{1 - u^2} \langle \mathbf{y}^*, \mathbf{z}^* \rangle \geq t) d\sigma_{d-1}(\mathbf{z}^*) ds. \end{aligned}$$

If $u > -1$ then this reduces to (2.5). For $u = -1$ we get

$$V_2(u; t, d) = \frac{\omega_{d-1}}{\omega_d} \int_{-1}^1 \mathbf{1}(s \geq t) \mathbf{1}(-s \geq t) (1 - s^2)^{\frac{d}{2}-1} ds.$$

which reduces to (2.6). \square

When we give probabilistic arguments and interpretations we do so for a random center \mathbf{y} of a spherical cap. We use Models 1 and 2 below. Model 1 is illustrated in Figure 1. Model 2 is illustrated in Figure 2 of Section 4 where we first use it.

Model 1. *The vector \mathbf{y} is uniformly distributed on the sphere \mathbb{S}^d . Expectation under this model is denoted $\mathbb{E}_1(\cdot)$.*

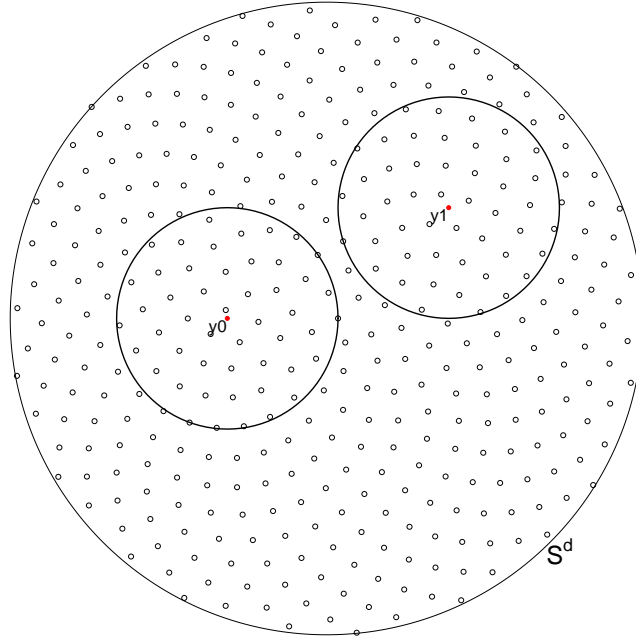


Fig 1: Illustration for Model 1. The point \mathbf{y} is uniformly distributed over \mathbb{S}^d . The small open circles represent permuted vectors \mathbf{x}_k . The point \mathbf{y}_0 is the observed value of \mathbf{y} . The circle around it goes through \mathbf{x}_0 and represents a spherical cap of height $\mathbf{y}_0^\top \mathbf{x}_0$. A second spherical cap of equal volume is centered at $\mathbf{y} = \mathbf{y}_1$. We study moments of $p(\mathbf{y}; \hat{\rho})$, the fraction of \mathbf{x}_k in the cap centered at random \mathbf{y} .

Model 2. *The vector \mathbf{y} is uniformly distributed on $\{\mathbf{z} \in \mathbb{S}^d \mid \mathbf{z}^\top \mathbf{x}_c = \tilde{\rho}\}$, for some $-1 \leq \tilde{\rho} \leq 1$, and $c \in \{0, 1, \dots, N-1\}$. Then $\mathbf{y} = \tilde{\rho} \mathbf{x}_c + \sqrt{1 - \tilde{\rho}^2} \mathbf{y}^*$ for \mathbf{y}^* uniformly distributed on a subset of \mathbb{S}^d isometric to \mathbb{S}^{d-1} . Expectation under this model is denoted $\mathbb{E}_2(\cdot)$.*

3. Approximation via spherical cap volume

Here we study the approximate p -value $\hat{p}_1(\hat{\rho}) = \sigma_d(C(\mathbf{y}; \hat{\rho}))$. First we find the mean squared error of this approximation over all spherical caps of the given volume via invariance. Then we give a probabilistic interpretation which includes the conditional unbiasedness result in Proposition 2 below. Then we give two computational simplifications, first for points obtained via permutation, and second for permutations of a binary vector. We begin by restating the invariance principle.

Theorem 1. Let $\mathbf{x}_0, \dots, \mathbf{x}_{N-1}$ be any points in \mathbb{S}^d . Then

$$\begin{aligned} \frac{1}{N^2} \sum_{k,l=0}^{N-1} \|\mathbf{x}_k - \mathbf{x}_l\| + \frac{1}{C_d} \int_{-1}^1 \int_{\mathbb{S}^d} \left| \sigma_d(C(\mathbf{z}; t)) - \frac{1}{N} \sum_{k=0}^{N-1} \mathbf{1}_{C(\mathbf{z}; t)}(\mathbf{x}_k) \right|^2 d\sigma_d(\mathbf{z}) dt \\ = \int_{\mathbb{S}^d} \int_{\mathbb{S}^d} \|\mathbf{x} - \mathbf{y}\| d\sigma_d(\mathbf{x}) d\sigma_d(\mathbf{y}) \end{aligned}$$

where $C_d = \omega_{d-1}/(d\omega_d)$.

Proof. Stolarsky (1973). \square

Brauchart and Dick (2013) gave a simple proof of Theorem 1 using reproducing kernel Hilbert spaces. They generalized Theorem 1 as follows.

Theorem 2. Let $\mathbf{x}_0, \dots, \mathbf{x}_{N-1}$ be any points in \mathbb{S}^d . Let $v : [-1, 1] \rightarrow (0, \infty)$ be any function with an antiderivative. Then

$$\begin{aligned} & \int_{-1}^1 v(t) \int_{\mathbb{S}^d} \left| \sigma_d(C(\mathbf{z}; t)) - \frac{1}{N} \sum_{k=0}^{N-1} \mathbf{1}_{C(\mathbf{z}; t)}(\mathbf{x}_k) \right|^2 d\sigma_d(\mathbf{z}) dt \\ &= \frac{1}{N^2} \sum_{k,l=0}^{N-1} K_v(\mathbf{x}_k, \mathbf{x}_l) - \int_{\mathbb{S}^d} \int_{\mathbb{S}^d} K_v(\mathbf{x}, \mathbf{y}) d\sigma_d(\mathbf{x}) d\sigma_d(\mathbf{y}) \end{aligned} \quad (3.1)$$

where $K_v(\mathbf{x}, \mathbf{y})$ is a reproducing kernel function defined by

$$K_v(\mathbf{x}, \mathbf{y}) = \int_{-1}^1 v(t) \int_{\mathbb{S}^d} \mathbf{1}_{C(\mathbf{z}; t)}(\mathbf{x}) \mathbf{1}_{C(\mathbf{z}; t)}(\mathbf{y}) d\sigma_d(\mathbf{z}) dt. \quad (3.2)$$

Proof. See Theorem 5.1 in Brauchart and Dick (2013). \square

If we set $v(t) = 1$ and $K(\mathbf{x}, \mathbf{y}) = 1 - C_d \|\mathbf{x} - \mathbf{y}\|$, then we recover the original Stolarsky formula. Note that the statement of Theorem 5.1 in Brauchart and Dick (2013) has a sign error in their counterpart to (3.1). The corrected statement (3.1) can be verified by comparing equations (5.3) and (5.4) of Brauchart and Dick (2013).

We would like a version of (3.1) just for one value of t such as $t = \hat{\rho} = \mathbf{x}_0^\top \mathbf{y}_0$. For $\hat{\rho} \in [-1, 1)$ and $\epsilon = (\epsilon_1, \epsilon_2) \in (0, 1)^2$, let

$$v_\epsilon(t) = \epsilon_2 + \frac{1}{\epsilon_1} \mathbf{1}(\hat{\rho} \leq t \leq \hat{\rho} + \epsilon_1). \quad (3.3)$$

Each v_ϵ satisfies the conditions of Theorem 2 making (3.1) an identity in ϵ . We let $\epsilon_2 \rightarrow 0$ and then $\epsilon_1 \rightarrow 0$ on both sides of (3.1) for $v = v_\epsilon$ yielding Theorem 3.

Theorem 3. Let $\mathbf{x}_0, \mathbf{x}_1, \dots, \mathbf{x}_N \in \mathbb{S}^d$ and $t \in [-1, 1]$. Then

$$\int_{\mathbb{S}^d} |p(\mathbf{y}, t) - \hat{p}_1(t)|^2 d\sigma_d(\mathbf{y}) = \frac{1}{N^2} \sum_{k=0}^{N-1} \sum_{l=0}^{N-1} \sigma_d(C_2(\mathbf{x}_k, \mathbf{x}_l; t)) - \hat{p}_1(t)^2. \quad (3.4)$$

Proof. See Section 10.1 of the Appendix which uses the limit argument described above. \square

We now give a proposition that holds for all models, including our Model 1 and Model 2.

Proposition 1. *For a random point $\mathbf{y} \in \mathbb{S}^d$,*

$$\mathbb{E}(p(\mathbf{y}, t)) = \frac{1}{N} \sum_{k=0}^{N-1} \Pr(\mathbf{y} \in C(\mathbf{x}_k; t)), \quad \text{and} \quad (3.5)$$

$$\mathbb{E}(p(\mathbf{y}, t)^2) = \frac{1}{N^2} \sum_{k,l=0}^{N-1} \Pr(\mathbf{y} \in C_2(\mathbf{x}_k, \mathbf{x}_l; t)). \quad (3.6)$$

Proposition 1 provides a probabilistic interpretation for equation (3.4). When $\mathbf{y} \sim \mathbf{U}(\mathbb{S}^d)$, the double sum on right side of (3.4) is $\mathbb{E}(p(\mathbf{y}, t)^2)$. Additionally $\hat{p}_1(t)$ has a probabilistic interpretation under Model 1.

Proposition 2. *For any $\mathbf{x}_0, \dots, \mathbf{x}_{N-1} \in \mathbb{S}^d$ and $t \in [-1, 1]$, $\hat{p}_1(t) = \mathbb{E}_1(p(\mathbf{y}, t))$.*

Proof. $\mathbb{E}_1(p(\mathbf{y}, t)) = \mathbb{E}_1 \left[\frac{1}{N} \sum_{k=0}^{N-1} \mathbf{1}_{C(\mathbf{y}; t)}(\mathbf{x}_k) \right] = \sigma_d(C_d(\mathbf{y}; t)) = \hat{p}_1(t).$ \square

Combining Proposition 2 and Theorem 3 we find that if $\mathbf{y} \sim \mathbf{U}(\mathbb{S}^d)$, as it would for IID Gaussian Y_i , then $p(\mathbf{y}, \hat{\rho})$ is a random variable with mean $\hat{p}_1(\hat{\rho})$ and variance given by (3.4) with $t = \hat{\rho}$.

The right hand side of (3.4) sums $O(N^2)$ terms. In a permutation analysis we might have $N = n!$ or $N = \binom{m_0+m_1}{m_0}$ for binary X_i , and so the computational cost could be high. The symmetry in a permutation set allows us to use

$$\int_{\mathbb{S}^d} |p(\mathbf{y}, t) - \hat{p}_1(t)|^2 d\sigma_d(\mathbf{y}) = \frac{1}{N} \sum_{k=0}^{N-1} \sigma_d(C_2(\mathbf{x}_0, \mathbf{x}_k; t)) - \hat{p}_1(t)^2$$

instead. But that costs $O(N)$, the same as the full permutation analysis.

When the X_i are binary, then for fixed t , $\sigma_d(C_2(\mathbf{x}_k, \mathbf{x}_l; t))$ just depends on the swap distance r between \mathbf{x}_k and \mathbf{x}_l . Then

$$\int_{\mathbb{S}^d} |p(\mathbf{y}, t) - \hat{p}_1(t)|^2 d\sigma_d(\mathbf{y}) = \frac{1}{N} \sum_{r=0}^m N_r V_2(u(r); t, d) - \hat{p}_1(t)^2 \quad (3.7)$$

for $V_2(u(r); t, d)$ given in Lemma 1 and $N_r = \sum_{k=0}^{N-1} \sum_{l=0}^{N-1} \mathbf{1}(r_{k,l} = r)$ counts pairs $(\mathbf{x}_k, \mathbf{x}_l)$ at swap distance r .

Theorem 4. *Let $\mathbf{x}_0 \in \mathbb{S}^d$ be the centered and scaled vector from an experiment with binary X_i of which m_0 are negative and m_1 are positive. Let $\mathbf{x}_0, \mathbf{x}_1, \dots, \mathbf{x}_{N-1}$ be the $N = \binom{m_0+m_1}{m_0}$ distinct permutations of \mathbf{x}_0 . If $\mathbf{y} \sim \mathbf{U}(\mathbb{S}^d)$, then for*

$t \in [-1, 1]$, and with $u(r)$ defined in (2.2),

$$\begin{aligned}\mathbb{E}(p(\mathbf{y}; t)) &= \sigma_d(C(\mathbf{y}_0; t)), \quad \text{and} \\ \text{Var}(p(\mathbf{y}, t)) &= \frac{1}{N} \sum_{r=0}^m \binom{m_0}{r} \binom{m_1}{r} V_2(u(r); t, d) - \hat{p}_1(t)^2.\end{aligned}$$

Proof. There are $\binom{m_0}{r} \binom{m_1}{r}$ permuted points \mathbf{x}_i at swap distance r from \mathbf{x}_0 . \square

4. A finer approximation to the p -value

In the previous section, we studied the distribution of p -values with the spherical cap centers \mathbf{y} uniformly distributed on the sphere \mathbb{S}^d . In this section, we give a finer approximation to $p(\mathbf{y}_0, \hat{\rho})$ by studying the distribution of the p -values with centers \mathbf{y} satisfying the constraint $\langle \mathbf{y}, \mathbf{x}_c \rangle = \langle \mathbf{y}_0, \mathbf{x}_c \rangle = \tilde{\rho}$. The point \mathbf{x}_c may be any permutation of \mathbf{x}_0 . There are two special choices. The first is to choose $c = 0$ so that $\mathbf{x}_c = \mathbf{x}_0$ is the original unpermuted data. The second is to choose \mathbf{x}_c to be the closest permutation of \mathbf{x}_0 to \mathbf{y}_0 . That is $c = \arg \max_i \langle \mathbf{y}_0, \mathbf{x}_i \rangle$. We will give a general formula that works for any choice of \mathbf{x}_c and compare the performance of the above two choices.

The rationale for conditioning on all \mathbf{y} satisfying $\langle \mathbf{y}, \mathbf{x}_c \rangle = \tilde{\rho}$ is as follows. Since we want the exact p -value centered at \mathbf{y}_0 with radius $\hat{\rho}$, the more targeted set of p -values we study, the better our approximation should be. When conditioning on $\langle \mathbf{y}, \mathbf{x}_c \rangle = \tilde{\rho}$, we eliminate many irrelevant \mathbf{y} . The approximation could be improved by conditioning on even more information, but the cost would go up. If we condition on the order statistic of all inner products $\langle \mathbf{y}_0, \mathbf{x}_i \rangle$, we get back the exact p -value.

For an index $c \in \{0, 1, \dots, N-1\}$ we propose finer approximations to the p -value based on Model 2 from Section 2. These are

$$\tilde{p}_c = \mathbb{E}_2(p(\mathbf{y}, \hat{\rho})) = \mathbb{E}_1(p(\mathbf{y}, \hat{\rho}) \mid \mathbf{y}^\top \mathbf{x}_c = \mathbf{y}_0^\top \mathbf{x}_c). \quad (4.1)$$

We are interested in two special cases,

$$\hat{p}_2 = \tilde{p}_0, \quad \text{and} \quad \hat{p}_3 = \tilde{p}_c, \quad \text{where} \quad c = \arg \max_{0 \leq i < N} \langle \mathbf{y}_0, \mathbf{x}_i \rangle. \quad (4.2)$$

For an illustration of Model 2 see Figure 2.

Notice that \hat{p}_2 cannot go below $1/N$ because all of the points \mathbf{y} that it includes have $\mathbf{x}_0 \in C(\mathbf{y}; \hat{\rho})$. In fact \mathbf{x}_0 is on the boundary of this spherical cap. Since the true value satisfies $p \geq 1/N$, having $\hat{p}_2 \geq 1/N$ is a desirable property. Similarly, $\hat{p}_3 \geq 1/N$ because then \mathbf{x}_c is in general an interior point of $C(\mathbf{y}, \hat{\rho})$. We expect that \hat{p}_3 should be more conservative than \hat{p}_2 and we see this numerically in Section 7.

From Proposition 1, we can get our estimate \tilde{p}_c and its mean squared error by finding single and double inclusion probabilities for \mathbf{y} .

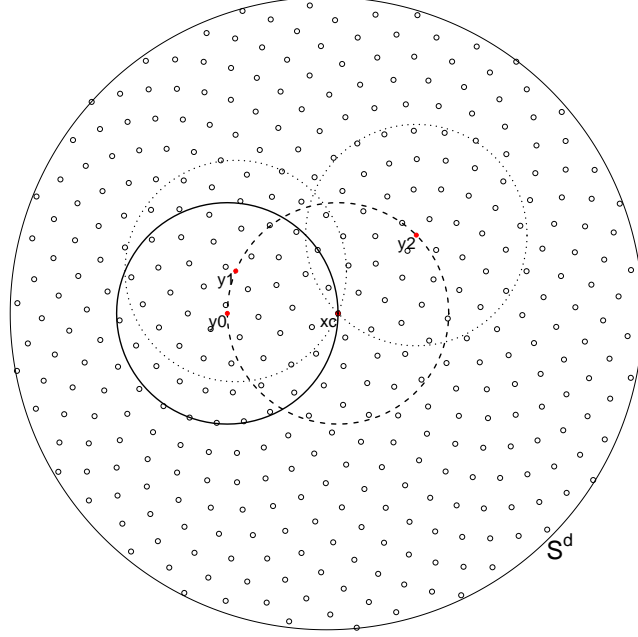


Fig 2: Illustration for Model 2. The original response vector is \mathbf{y}_0 with $\mathbf{y}_0^\top \mathbf{x}_0 = \hat{\rho}$. We consider alternative \mathbf{y} uniformly distributed on the surface of $C(\mathbf{x}_0; \hat{\rho})$ with examples \mathbf{y}_1 and \mathbf{y}_2 . Around each such \mathbf{y}_j there is a spherical cap of height $\hat{\rho}$ that just barely includes $\mathbf{x}_c = \mathbf{x}_0$. We use $\hat{p}_2 = \mathbb{E}_2(p(\mathbf{y}; \hat{\rho}))$ and find an expression for $\mathbb{E}_2((\hat{p}_2 - p(\mathbf{y}; \hat{\rho}))^2)$.

To compute \tilde{p}_c we need to sum N values $\Pr(\mathbf{y} \in C(\mathbf{x}_k; t) \mid \mathbf{y}^\top \mathbf{x}_c = \tilde{\rho})$ and for \tilde{p}_c to be useful we must compute it in $o(N)$ time. The computations are feasible in the binary case, which we now focus on.

Let $u_j = \mathbf{x}_j^\top \mathbf{x}_0$ for $j = 1, 2$, and let $u_3 = \mathbf{x}_1^\top \mathbf{x}_2$. Let the projection of \mathbf{y} on \mathbf{x}_c be $\mathbf{y} = \tilde{\rho} \mathbf{x}_c + \sqrt{1 - \tilde{\rho}^2} \mathbf{y}^*$. Then the single and double point inclusion probabilities under Model 2 are

$$P_1(u_1, \tilde{\rho}, \hat{\rho}) = \int_{\mathbb{S}^{d-1}} \mathbf{1}(\langle \mathbf{y}, \mathbf{x}_1 \rangle \geq \hat{\rho}) d\sigma_{d-1}(\mathbf{y}^*), \quad \text{and} \quad (4.3)$$

$$P_2(u_1, u_2, u_3, \tilde{\rho}, \hat{\rho}) = \int_{\mathbb{S}^{d-1}} \mathbf{1}(\langle \mathbf{y}, \mathbf{x}_1 \rangle \geq \hat{\rho}) \mathbf{1}(\langle \mathbf{y}, \mathbf{x}_2 \rangle \geq \hat{\rho}) d\sigma_{d-1}(\mathbf{y}^*) \quad (4.4)$$

where $\hat{\rho} = \langle \mathbf{x}_0, \mathbf{y}_0 \rangle$. If two permutations of \mathbf{x}_0 are at swap distance r , then their inner product is $u(r) = 1 - r(m_0^{-1} + m_1^{-1})$ from equation (2.2).

Lemma 2. *Let the projection of \mathbf{x}_1 onto \mathbf{x}_c be $\mathbf{x}_1 = u_1 \mathbf{x}_c + \sqrt{1 - u_1^2} \mathbf{x}_1^*$. Then*

the single point inclusion probability from (4.3) is

$$P_1(u_1, \tilde{\rho}, \hat{\rho}) = \begin{cases} \mathbf{1}(\tilde{\rho}u_1 \geq \hat{\rho}), & u_1 = \pm 1 \text{ or } \tilde{\rho} = \pm 1 \\ \sigma_{d-1}(C(\mathbf{x}_1^*, \rho^*)), & u_1 \in (-1, 1), \tilde{\rho} \in (-1, 1) \end{cases} \quad (4.5)$$

where $\rho^* = (\hat{\rho} - \tilde{\rho}u_1)/\sqrt{(1 - \tilde{\rho}^2)(1 - u_1^2)}$.

Proof. The projection of \mathbf{y} onto \mathbf{x}_c is $\mathbf{y} = \tilde{\rho}\mathbf{x}_c + \sqrt{1 - \tilde{\rho}^2}\mathbf{y}^*$. Now

$$\langle \mathbf{y}, \mathbf{x}_1 \rangle = \begin{cases} \tilde{\rho}u_1, & u_1 = \pm 1 \text{ or } \tilde{\rho} = \pm 1 \\ \tilde{\rho}u_1 + \sqrt{1 - \tilde{\rho}^2}\sqrt{1 - u_1^2}\langle \mathbf{y}^*, \mathbf{x}_1^* \rangle, & u_1 \in (-1, 1), \tilde{\rho} \in (-1, 1) \end{cases}$$

and the result easily follows. \square

We can now give a computable expression for \tilde{p}_c and hence for \hat{p}_2 and \hat{p}_3 .

Theorem 5. For $-1 \leq \hat{\rho} \leq 1$, $-1 \leq \tilde{\rho} \leq 1$,

$$\tilde{p}_c = \mathbb{E}_2(p(\mathbf{y}, \hat{\rho})) = \frac{1}{N} \sum_{r=0}^m \binom{m_0}{r} \binom{m_1}{r} P_1(u(r), \tilde{\rho}, \hat{\rho}) \quad (4.6)$$

where $u(r)$ is given in equation (2.2), $P_1(u(r), \tilde{\rho}, \hat{\rho})$ is given in equation (4.5) and $\tilde{\rho} = \mathbf{x}_c^T \mathbf{y}_0$.

Proof. There are $\binom{m_0}{r} \binom{m_1}{r}$ permutations of \mathbf{x}_0 at swap distance r from \mathbf{x}_c . \square

From (4.6) we see that \tilde{p}_c can be computed in $O(m)$ work. The mean squared error for \tilde{p}_c is more complicated and will be more expensive. We need the double point inclusion probabilities and then we need to count the number of pairs $\mathbf{x}_k, \mathbf{x}_l$ forming a given set of swap distances among $\mathbf{x}_k, \mathbf{x}_l, \mathbf{x}_c$.

Lemma 3. For $j = 1, 2$, let \mathbf{x}_j be at swap distance r_j from \mathbf{x}_c and let r_3 be the swap distance between \mathbf{x}_1 and \mathbf{x}_2 . Let u_1, u_2, u_3 be the corresponding inner products given by (2.2). If there are equalities among $\mathbf{x}_1, \mathbf{x}_2$ and \mathbf{x}_c , then the double point inclusion probability from (4.4) is

$$P_2(u_1, u_2, u_3, \tilde{\rho}, \hat{\rho}) = \begin{cases} \mathbf{1}(\tilde{\rho} \geq \hat{\rho}), & \mathbf{x}_1 = \mathbf{x}_2 = \mathbf{x}_c \\ \mathbf{1}(\tilde{\rho} \geq \hat{\rho})P_1(u_2, \tilde{\rho}, \hat{\rho}), & \mathbf{x}_1 = \mathbf{x}_c \neq \mathbf{x}_2 \\ \mathbf{1}(\tilde{\rho} \geq \hat{\rho})P_1(u_1, \tilde{\rho}, \hat{\rho}), & \mathbf{x}_2 = \mathbf{x}_c \neq \mathbf{x}_1 \\ P_1(u_2, \tilde{\rho}, \hat{\rho}), & \mathbf{x}_1 = \mathbf{x}_2 \neq \mathbf{x}_c. \end{cases}$$

If $\mathbf{x}_1, \mathbf{x}_2$ and \mathbf{x}_c are three distinct points with $\min(u_1, u_2) = -1$, then

$$P_2(u_1, u_2, u_3, \tilde{\rho}, \hat{\rho}) = \begin{cases} \mathbf{1}(-\tilde{\rho} \geq \hat{\rho})P_1(u_2, \tilde{\rho}, \hat{\rho}), & u_1 = -1 \\ \mathbf{1}(-\tilde{\rho} \geq \hat{\rho})P_1(u_1, \tilde{\rho}, \hat{\rho}), & u_2 = -1. \end{cases}$$

$$\begin{aligned}
\mathbf{x}_c &= (\overbrace{+, +, +, +, +, \dots, +, +, +, +}^{m_1}, \overbrace{-, -, -, -, \dots, -, -, -, -}^{m_0}) \\
\mathbf{x}_1 &= (\overbrace{+, +, +, \dots, +, \underbrace{-, -, -, \dots, -}_{r_1}}^{m_1}, \overbrace{+, +, +, \dots, +, +, +, -}^{m_0}) \\
\mathbf{x}_2 &= (\overbrace{+, \dots, +, \underbrace{-, \dots, -}_{\delta_1}}^{m_1}, \overbrace{-, \dots, -, \underbrace{+, +, \dots, +, -}_{\delta_2}, \dots, -}^{m_0})
\end{aligned}$$

Fig 3: Illustration of r_1 , r_2 , δ_1 and δ_2 . The points \mathbf{x}_c , \mathbf{x}_1 and \mathbf{x}_2 each have m_0 negative and m_1 positive components. For $j = 1, 2$ the swap distance between \mathbf{x}_j and \mathbf{x}_c is r_j . There are δ_1 positive components of \mathbf{x}_c where both \mathbf{x}_1 and \mathbf{x}_2 are negative, and δ_2 negative components of \mathbf{x}_c where both \mathbf{x}_1 and \mathbf{x}_2 are positive.

Otherwise $-1 < u_1, u_2 < 1$, and then

$$\begin{aligned}
P_2(u_1, u_2, u_3, \tilde{\rho}, \hat{\rho}) \\
= \begin{cases} \mathbf{1}(\tilde{\rho}u_1 \geq \hat{\rho})\mathbf{1}(\tilde{\rho}u_2 \geq \hat{\rho}), & \tilde{\rho} = \pm 1 \\ \int_{-1}^1 \frac{\omega_{d-2}}{\omega_{d-1}}(1-t^2)^{\frac{d-1}{2}-1} \mathbf{1}(t \geq \rho_1) \mathbf{1}(tu_3^* \geq \rho_2) dt, & \tilde{\rho} \neq \pm 1, u_3^* = \pm 1 \\ \int_{-1}^1 \frac{\omega_{d-2}}{\omega_{d-1}}(1-t^2)^{\frac{d-1}{2}-1} \mathbf{1}(t \geq \rho_1) \sigma_{d-2}(C(\mathbf{x}_2^{**}, \frac{\rho_2 - tu_3^*}{\sqrt{1-t^2}\sqrt{1-u_3^{*2}}})) dt, & \tilde{\rho} \neq \pm 1, |u_3^*| < 1 \end{cases}
\end{aligned}$$

where

$$u_3^* = \frac{u_3 - u_1 u_2}{\sqrt{1-u_1^2}\sqrt{1-u_2^2}} \quad \text{and} \quad \rho_j = \frac{\hat{\rho} - \tilde{\rho}u_j}{\sqrt{1-\tilde{\rho}^2}\sqrt{1-u_j^2}}, \quad j = 1, 2 \quad (4.7)$$

and \mathbf{x}_2^{**} is the residual from the projection of \mathbf{x}_2^* on \mathbf{x}_1^* .

Proof. See Section 10.2. □

Next we consider the swap configuration among \mathbf{x}_1 , \mathbf{x}_2 and \mathbf{x}_c . Let \mathbf{x}_j be at swap distance r_j from \mathbf{x}_c , for $j = 1, 2$. We let δ_1 be the number of positive components of \mathbf{x}_c that are negative in both \mathbf{x}_1 and \mathbf{x}_2 . Similarly, δ_2 is the number of negative components of \mathbf{x}_c that are positive in both \mathbf{x}_1 and \mathbf{x}_2 . See Figure 3. The swap distance between \mathbf{x}_1 and \mathbf{x}_2 is then $r_3 = r_1 + r_2 - \delta_1 - \delta_2$.

Let $\mathbf{r} = (r_1, r_2)$, $\boldsymbol{\delta} = (\delta_1, \delta_2)$ and $\underline{r} = \min(r_1, r_2)$. We will study values of $r_1, r_2, r_3, \delta_1, \delta_2$ ranging over the following sets:

$$\begin{aligned}
r_1, r_2 &\in R = \{1, \dots, \underline{m}\} \\
\delta_1 &\in D_1(\mathbf{r}) = \{\max(0, r_1 + r_2 - m_0), \dots, \underline{r}\} \\
\delta_2 &\in D_2(\mathbf{r}) = \{\max(0, r_1 + r_2 - m_1), \dots, \underline{r}\}, \quad \text{and} \\
r_3 &\in R_3(\mathbf{r}) = \{\max(1, r_1 + r_2 - 2\underline{r}), \dots, \min(r_1 + r_2, \underline{m}, m_0 + m_1 - r_1 - r_2)\}.
\end{aligned}$$

Whenever the lower bound for one of these sets exceeds the upper bound, we take the set to be empty, and a sum over it to be zero. Note that while $r_1 = 0$ is possible, it corresponds to $\mathbf{x}_1 = \mathbf{x}_c$ and we will handle that case specially, excluding it from R .

The number of pairs $(\mathbf{x}_l, \mathbf{x}_k)$ with a fixed \mathbf{r} and $\boldsymbol{\delta}$ is

$$c(\mathbf{r}, \boldsymbol{\delta}) = \binom{m_0}{\delta_1} \binom{m_1}{\delta_2} \binom{m_0 - \delta_1}{r_1 - \delta_1} \binom{m_1 - \delta_2}{r_1 - \delta_2} \binom{m_0 - r_1}{r_2 - \delta_1} \binom{m_1 - r_1}{r_2 - \delta_2}. \quad (4.8)$$

Then the number of configurations given r_1 , r_2 and r_3 is

$$c(r_1, r_2, r_3) = \sum_{\delta_1 \in D_1} \sum_{\delta_2 \in D_2} c(\mathbf{r}, \boldsymbol{\delta}) \mathbf{1}(r_3 = r_1 + r_2 - \delta_1 - \delta_2). \quad (4.9)$$

We can now get an expression for the expected mean squared under Model 2 which combined with Theorem 5 for the mean provides an expression for the mean squared error of \tilde{p}_c .

Theorem 6. *For $-1 \leq \hat{\rho} \leq 1, -1 \leq \tilde{\rho} \leq 1$,*

$$\begin{aligned} \mathbb{E}_2(p(\mathbf{y}, \hat{\rho})^2) &= \frac{1}{N^2} \left[\mathbf{1}(\tilde{\rho} \geq \hat{\rho}) + 2 \sum_{r=1}^m \binom{m_0}{r} \binom{m_1}{r} P_2(1, u(r), u(r), \tilde{\rho}, \hat{\rho}) \right. \\ &\quad + \sum_{r=1}^m \binom{m_0}{r} \binom{m_1}{r} P_1(u(r), \tilde{\rho}, \hat{\rho}) \\ &\quad \left. + \sum_{r_1 \in R} \sum_{r_2 \in R} \sum_{r_3 \in R_3(\mathbf{r})} c(r_1, r_2, r_3) P_2(u_1, u_2, u_3, \tilde{\rho}, \hat{\rho}) \right] \end{aligned} \quad (4.10)$$

where $P_2(\cdot)$ is the double inclusion probability in (4.4) and $c(r_1, r_2, r_3)$ is the configuration count in (4.9).

Proof. See Section 10.3 of the Appendix. \square

In our experience, the cost of computing $\mathbb{E}_2(p(\mathbf{y}, \hat{\rho})^2)$ under Model 2 is dominated by the cost of the $O(\underline{m}^3)$ integrals required to get the $P_2(\cdot)$ values in (4.10). The cost also includes an $O(\underline{m}^4)$ component because $c(r_1, r_2, r_3)$ is also a sum of $O(\underline{m})$ terms, but it did not dominate the computation at the sample sizes we looked at (up to several hundred).

5. Generalized Stolarsky Invariance

Here we obtain the Model 2 results in a different way, by extending the work by Brauchart and Dick (2013). They introduced a weight on the height t of the spherical cap in the average. We now apply a weight function to the inner product $\langle \mathbf{z}, \mathbf{x}_c \rangle$ between the center \mathbf{z} of the spherical cap and a special point \mathbf{x}_c .

Theorem 7. Let $\mathbf{x}_0, \dots, \mathbf{x}_{N-1}$ be arbitrary points in \mathbb{S}^d and $v(\cdot)$ and $h(\cdot)$ be positive functions in $L_2([-1, 1])$. Then for any $\mathbf{x}' \in \mathbb{S}^d$, the following equation holds,

$$\begin{aligned} & \int_{-1}^1 v(t) \int_{\mathbb{S}^d} h(\langle \mathbf{z}, \mathbf{x}' \rangle) \left| \sigma_d(C(\mathbf{z}; t)) - \frac{1}{N} \sum_{k=0}^{N-1} \mathbf{1}_{C(\mathbf{z}; t)}(\mathbf{x}_k) \right|^2 d\sigma_d(\mathbf{z}) dt \\ &= \frac{1}{N^2} \sum_{k,l=0}^{N-1} K_{v,h,\mathbf{x}'}(\mathbf{x}_k, \mathbf{x}_l) + \int_{\mathbb{S}^d} \int_{\mathbb{S}^d} K_{v,h,\mathbf{x}'}(\mathbf{x}, \mathbf{y}) d\sigma_d(\mathbf{x}) d\sigma_d(\mathbf{y}) \\ & \quad - \frac{2}{N} \sum_{k=0}^{N-1} \int_{\mathbb{S}^d} K_{v,h,\mathbf{x}'}(\mathbf{x}, \mathbf{x}_k) d\sigma_d(\mathbf{x}) \end{aligned} \quad (5.1)$$

where $K_{v,h,\mathbf{x}'} : \mathbb{S}^d \times \mathbb{S}^d \rightarrow \mathbb{R}$ is a reproducing kernel defined by

$$K_{v,h,\mathbf{x}'}(\mathbf{x}, \mathbf{y}) = \int_{-1}^1 v(t) \int_{\mathbb{S}^d} h(\langle \mathbf{z}, \mathbf{x}' \rangle) \mathbf{1}_{C(\mathbf{z}; t)}(\mathbf{x}) \mathbf{1}_{C(\mathbf{z}; t)}(\mathbf{y}) d\sigma_d(\mathbf{z}) dt. \quad (5.2)$$

Proof. See Section 10.4 of the Appendix. \square

Remark. We will use this result for $\mathbf{x}' = \mathbf{x}_c$, where \mathbf{x}_c is one of the N given points. The theorem holds for general $\mathbf{x}' \in \mathbb{S}^d$, but the result is computationally and statistically more attractive when $\mathbf{x}' = \mathbf{x}_c$.

We now show that the second moment in Theorem 6 holds as a special limiting case of Theorem 7. In addition to v_ϵ from Section 3 we introduce $\boldsymbol{\eta} = (\eta_1, \eta_2) \in (0, 1)^2$ and

$$h_{\boldsymbol{\eta}}(s) = \eta_2 + \frac{1}{\eta_1 \left(\frac{\omega_{d-1}}{\omega_d} (1 - s^2)^{d/2-1} \right)} \mathbf{1}(\tilde{\rho} \leq s \leq \tilde{\rho} + \eta_1) \quad (5.3)$$

Using these results we can now establish the following theorem, which provides the second moment of $p(\mathbf{y}, \hat{\rho})$ under Model 2.

Theorem 8. Let $\mathbf{x}_0 \in \mathbb{S}^d$ be the centered and scaled vector from an experiment with binary X_i of which m_0 are negative and m_1 are positive. Let $\mathbf{x}_0, \mathbf{x}_1, \dots, \mathbf{x}_{N-1}$ be the $N = \binom{m_0+m_1}{m_0}$ distinct permutations of \mathbf{x}_0 . Let \mathbf{x}_c be one of the \mathbf{x}_k and let \tilde{p}_c be given by (4.1). Then

$$\mathbb{E}_2(p(\mathbf{y}, \hat{\rho})^2) = \frac{1}{N^2} \sum_{k,l=0}^{N-1} \int_{\mathbb{S}^{d-1}} \mathbf{1}(\langle \mathbf{y}, \mathbf{x}_k \rangle \geq \hat{\rho}) \mathbf{1}(\langle \mathbf{y}, \mathbf{x}_l \rangle \geq \hat{\rho}) d\sigma_{d-1}(\mathbf{y}^*)$$

where $\mathbf{y} = \tilde{\rho} \mathbf{x}_c + \sqrt{1 - \tilde{\rho}^2} \mathbf{y}^*$.

Proof. The proof uses Theorem 7 with a sequence of h defined in (5.3) and v defined in (3.3). See Section 10.5 of the appendix. \square

This result shows that we can use the invariance principle to derive the second moment of $p(\mathbf{y}, \hat{\rho})$ under Model 2. The mean square in Theorem 8 is consistent with the second moment equation (3.6) in Proposition 1.

6. Two sided p-values

In statistical applications it is more usual to report two-sided p -values. A conservative approach is to use $2 \min(p, 1 - p)$ where p is a one-sided p -value. A sharper choice is

$$p = \frac{1}{N} \sum_{k=0}^{N-1} \mathbf{1}(|\mathbf{x}_k^\top \mathbf{y}_0| \geq |\hat{\rho}|). \quad (6.1)$$

This choice changes our Model 2 estimate. It also changes the second moment of our Model 1 estimate.

The two-sided version of the estimate $\hat{p}_1(\hat{\rho})$ is $2\sigma_d(C(\mathbf{y}; |\hat{\rho}|))$, the same as if we had doubled a one-tailed estimate. Also $\mathbb{E}_1(p) = \hat{p}_1$ in the two tailed case. We now consider the mean square for the two-tailed estimate under Model 1. For $\mathbf{x}_1, \mathbf{x}_2 \in \mathbb{S}^d$ with $u = \mathbf{x}_1^\top \mathbf{x}_2$, the two-tailed double inclusion probability under Model 1 is

$$\tilde{V}_2(u; t, d) = \int_{\mathbb{S}^d} \mathbf{1}(|\mathbf{z}^\top \mathbf{x}_1| \geq |t|) \mathbf{1}(|\mathbf{z}^\top \mathbf{x}_2| \geq |t|) d\sigma_d(\mathbf{z}).$$

Writing $\mathbf{1}(|\mathbf{z}^\top \mathbf{x}_i| \geq |t|) = \mathbf{1}(\mathbf{z}^\top \mathbf{x}_i \geq |t|) + \mathbf{1}(\mathbf{z}^\top (-\mathbf{x}_i) \geq |t|)$ for $i = 1, 2$ and expanding the product, we get

$$\tilde{V}_2(u; t, d) = 2V_2(u; |t|, d) + 2V_2(-u; |t|, d).$$

By replacing $V_2(u, t, d)$ with $\tilde{V}_2(u, t, d)$ and $\hat{p}_1(t)$ with $2\sigma_d(C(\mathbf{y}; |t|))$ in Theorem 4, we get the variance of two-sided p-values under Model 1.

To obtain corresponding formulas under Model 2, we use the usual notations. Let $u_j = \mathbf{x}_j^\top \mathbf{x}_0$ for $j = 1, 2$, and let $u_3 = \mathbf{x}_1^\top \mathbf{x}_2$. Let the projection of \mathbf{y} on \mathbf{x}_c be $\mathbf{y} = \tilde{\rho} \mathbf{x}_c + \sqrt{1 - \tilde{\rho}^2} \mathbf{y}^*$. Now

$$\tilde{P}_1(u_1, \tilde{\rho}, \hat{\rho}) = \int_{\mathbb{S}^{d-1}} \mathbf{1}(|\langle \mathbf{y}, \mathbf{x}_1 \rangle| \geq |\hat{\rho}|) d\sigma_{d-1}(\mathbf{y}^*), \quad \text{and,} \quad (6.2)$$

$$\tilde{P}_2(u_1, u_2, u_3, \tilde{\rho}, \hat{\rho}) = \int_{\mathbb{S}^{d-1}} \mathbf{1}(|\langle \mathbf{y}, \mathbf{x}_1 \rangle| \geq |\hat{\rho}|) \mathbf{1}(|\langle \mathbf{y}, \mathbf{x}_2 \rangle| \geq |\hat{\rho}|) d\sigma_{d-1}(\mathbf{y}^*) \quad (6.3)$$

are the appropriate single and double inclusion probabilities.

After writing $\mathbf{1}(|\langle \mathbf{y}, \mathbf{x}_i \rangle| \geq |\hat{\rho}|) = \mathbf{1}(\langle \mathbf{y}, \mathbf{x}_i \rangle \geq |\hat{\rho}|) + \mathbf{1}(\langle \mathbf{y}, -\mathbf{x}_i \rangle \geq |\hat{\rho}|)$ for $i = 1, 2$ and expanding the product, we get

$$\begin{aligned} \tilde{P}_1(u_1, \tilde{\rho}, \hat{\rho}) &= P_1(u_1, \tilde{\rho}, |\hat{\rho}|) + P_1(-u_1, \tilde{\rho}, |\hat{\rho}|), \quad \text{and} \\ \tilde{P}_2(u_1, u_2, u_3, \tilde{\rho}, \hat{\rho}) &= P_2(u_1, u_2, u_3, \tilde{\rho}, |\hat{\rho}|) + P_2(-u_1, u_2, -u_3, \tilde{\rho}, |\hat{\rho}|) \\ &\quad + P_2(u_1, -u_2, -u_3, \tilde{\rho}, |\hat{\rho}|) + P_2(-u_1, -u_2, u_3, \tilde{\rho}, |\hat{\rho}|). \end{aligned}$$

Changing $P_1(u_1, \tilde{\rho}, \hat{\rho})$ and $P_2(u_1, u_2, u_3, \tilde{\rho}, \hat{\rho})$ to $\tilde{P}_1(u_1, \tilde{\rho}, \hat{\rho})$ and $\tilde{P}_2(u_1, u_2, u_3, \tilde{\rho}, \hat{\rho})$ respectively in Theorem 5 and 6, we get the first and second moments for two-sided p-values under Model 2.

For a two-sided p -value, \hat{p}_3 is calculated with \mathbf{x}_c where $\tilde{c} = \arg \max_i |\langle \mathbf{y}_0, \mathbf{x}_i \rangle|$. For $m_0 = m_1$, $\tilde{c} = c = \arg \max_i \langle \mathbf{y}_0, \mathbf{x}_i \rangle$, but the result may differ significantly for unequal sample sizes.

7. Numerical Results

We consider two-sided p -values in this section. First we evaluate the accuracy of \hat{p}_1 , the simple spherical cap volume approximate p value. We considered $m_0 = m_1$ in a range of values from 5 to 200. The values \hat{p}_1 ranged from just below 1 to 2×10^{-30} . We judge the accuracy of this estimate by its root mean squared error. Under Model 1 this is $(\mathbb{E}(\hat{p}_1(\rho) - p(\mathbf{y}, \rho))^2)^{1/2}$ for $\mathbf{y} \sim \mathbf{U}(\mathbb{S}^d)$. Figure 4a shows this RMSE decreasing towards 0 as \hat{p}_1 goes to 0 with ρ going to 1. The RMSE also decreases with increasing sample size, as we would expect from the central limit theorem.

As seen in Figures 4a and 4b, the RMSE is not monotone in \hat{p}_1 . Right at $\hat{p}_1 = 1$ we know that RMSE = 0 and around 0.1 there is a dip. The practically interesting values of \hat{p}_1 are much smaller than 0.1, and the RMSE is monotone for them.

A problem with \hat{p}_1 is that it can approach 0 even though $p \geq 1/N$. The Model 1 RMSE does not reflect this problem. By studying $\mathbb{E}_2((\hat{p}_1(\rho) - p(\mathbf{y}, \rho))^2)^{1/2}$, we get a different result. In Figure 4c, the RMSE of \hat{p}_1 under Model 2 reaches a plateau as \hat{p}_1 goes to 0. The Model 2 RMSE reveals the flaw in \hat{p}_1 going below $1/N$.

The estimator $\hat{p}_2 = \tilde{p}_0$ performs better than \hat{p}_1 because it makes more use of the data, and it is never below $1/N$. As seen in Figure 4d, the RMSE of \hat{p}_2 very closely matches \hat{p}_2 itself as \hat{p}_2 decreases to zero. That is, the relative error $|\hat{p}_2 - p|/\hat{p}_2$ is well behaved for small p -values. Also as \hat{p}_2 drops to the granularity limit $1/N$, its RMSE drops to 0.

The estimators \hat{p}_1 and \hat{p}_2 , do not differ much for larger p -values as seen in Figure 5a. But in the limit as $\hat{p} \rightarrow 1$ we see that $\hat{p}_1 \rightarrow 0$, while \hat{p}_2 approaches the granularity limit $1/N$ instead.

Figure 5b compares the RMSE of the two estimators under Model 2. As expected, \hat{p}_2 is more accurate. It also shows that the biggest differences occur only when \hat{p}_1 goes below $1/N$.

To examine the behavior of \hat{p}_2 more closely, we plot its coefficient of variation in Figure 6. We see that the relative uncertainty in \hat{p}_2 is not extremely large. Even when the estimated p -values are as small as 10^{-30} the coefficient of variation is below 5.

In Section 4, we mentioned another choice for \mathbf{x}_c . It was $\hat{p}_3 = \tilde{p}_c$, where \mathbf{x}_c is the closest permutation of \mathbf{x}_0 to \mathbf{y}_0 . We compare \hat{p}_3 to \hat{p}_2 in Figures 7 and 8. We fixed the observed \mathbf{x}_0 and ρ , and then randomly sampled 100 vectors \mathbf{y}_0 with $\langle \mathbf{y}_0, \mathbf{x}_0 \rangle = \rho$. All 100 of the \mathbf{y}_0 lead to the same value for \hat{p}_2 and its standard deviation. We get 100 different estimates for \hat{p}_3 and its standard deviation. We varied m_0 and m_1 , choosing ρ so that the values of \hat{p}_2 are comparable at different sample sizes. Figure 7 shows the estimates \hat{p}_3 with reference points for \hat{p}_2 . As expected \hat{p}_3 tends to be larger than \hat{p}_2 . Figure 8 shows the sample RMSEs for \hat{p}_3 with reference points for the RMSE for \hat{p}_2 . The top row of plots has $m_0 = m_1$ while the bottom row has $m_1 = 2m_0$. The left column of plots are at larger p -values than the rightmost column. We see that neither choice always has the smaller RMSE, but \hat{p}_2 is usually more accurate.

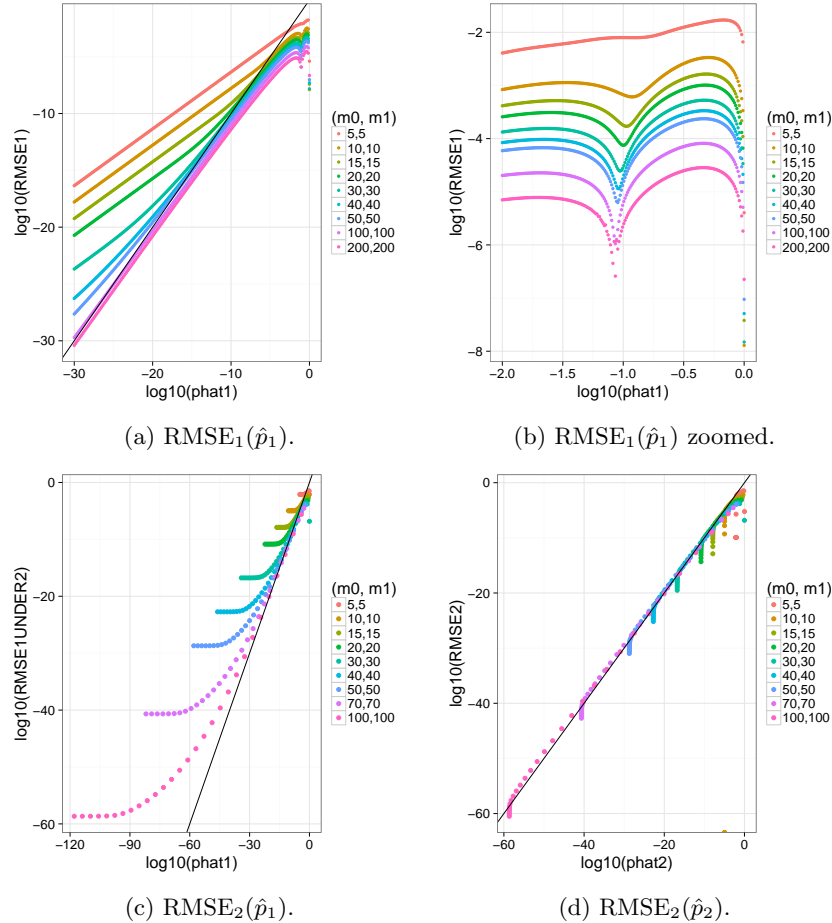


Fig 4: RMSEs for \hat{p}_1 and \hat{p}_2 under Models 1 and 2. The x -axis shows the estimate \hat{p} as ρ varies from 1 to 0. Here $m_0 = m_1$. Plots with $m_0 \neq m_1$ are similar.

8. Comparison to saddlepoint approximation

Many approximation methods have been proposed for permutation tests. Zhou et al. (2009) fit approximations by moments in the Pearson family. Larson and Owen (2015) fit Gaussian and beta approximations to linear statistics and gamma approximations to quadratic statistics for gene set testing problems. Knijnenburg et al. (2009) fit generalized extreme value distributions to the tails of sampled permutation values.

These approximations do not come with an all inclusive p -value that accounts for both numerical and sampling uncertainty. The sampling method does come with such a p -value if we add one to numerator and denominator as Barnard

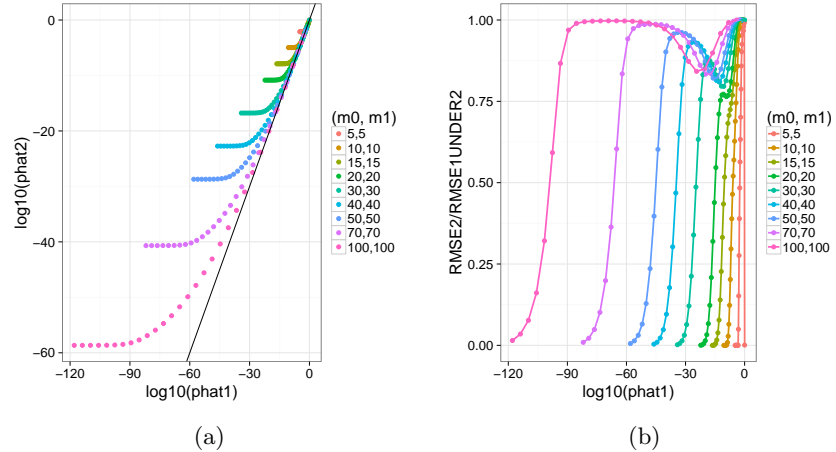


Fig 5: Comparison of \hat{p}_1 and \hat{p}_2 . In (a), $\log_{10}(\hat{p}_2)$ is plotted against $\log_{10}(\hat{p}_1)$ for varying ρ 's. The black line is the 45 degree line. In (b), the ratio of RMSEs for \hat{p}_1 and \hat{p}_2 is plotted against $\log_{10}(\hat{p}_1)$. The x -axis is $\log_{10}(\hat{p}_1)$.

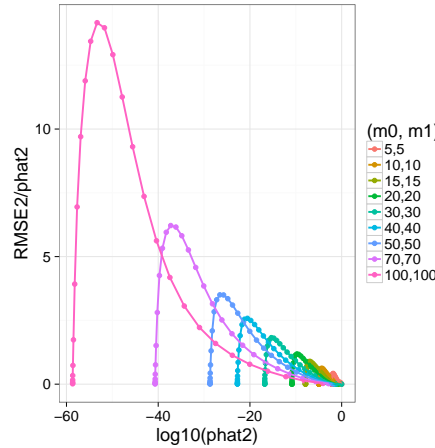


Fig 6: The coefficient of variation for \hat{p}_2 with varying ρ 's.

(1963) suggests. But that method cannot attain very small p -values. Reasonable power to attain $p \leq \epsilon$ requires a sample of somewhere between $3/\epsilon$ and $19/\epsilon$ random permutations (Larson and Owen, 2015).

The strongest theoretical support for approximate p -values comes from saddlepoint approximations. Reid (1988) surveys saddlepoint approximations and Robinson (1982) develops them for permutation tests of the linear statistics we have considered here. When the true p -value is p , the saddlepoint approximation

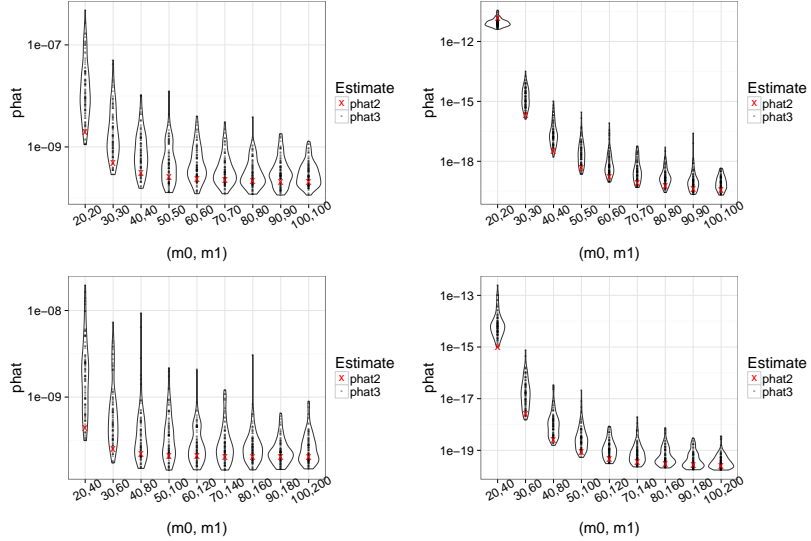


Fig 7: Comparison of \hat{p}_3 versus \hat{p}_2 . For a given triple $(m_0, m_1, \hat{\rho})$, we randomly sample 100 vectors \mathbf{y}_0 with $\mathbf{x}_0^\top \mathbf{y}_0 = \hat{\rho}$. By symmetry, \mathbf{x}_0 can be any permutation. We get 100 different \hat{p}_3 and a common \hat{p}_2 for each triple $(m_0, m_1, \hat{\rho})$. In the two panels on the left, $\hat{\rho}$'s are chosen to give two-sided $\hat{p}_1(\hat{\rho}) = 2 \times 10^{-10}$ with various dimensions (m_0, m_1) . The two panels on the right correspond to two-sided $\hat{p}_1(\hat{\rho}) = 2 \times 10^{-20}$. Estimates for two-sided p -values are plotted on the y -axis, with \hat{p}_3 plotted as black dots with distributions and \hat{p}_2 as red crosses.

\hat{p}_s satisfies $\hat{p}_s = p(1 + O(1/n))$. Because we do not know the implied constant in $O(1/n)$ or the n at which it takes effect, the saddlepoint approximation does not provide a computable upper bound for the true permutation p -value p .

Our approximations \hat{p}_2 and \hat{p}_3 have an RMSE of the same order of magnitude as the estimate itself. In this, they are much more accurate than \hat{p}_1 and comparable to saddlepoint approximations. We can get an upper bound for the p value with our method, under our model assumptions. Let $\mu = \mathbb{E}(p(\mathbf{y}, \hat{\rho}))$ and $\sigma^2 = \text{Var}(p(\mathbf{y}, \hat{\rho}))$ for the observed value $\hat{\rho} = \mathbf{x}_0^\top \mathbf{y}_0$ and for random \mathbf{y} under either Model 1 or 2. Then $\Pr(p \geq \mu + \lambda\sigma) \leq 1/(1 + \lambda^2)$ for any $\lambda > 0$. Under this model, $p^* = \mu + \lambda\sigma + 1/(1 + \lambda^2)$ is a conservative p -value. Minimizing that bound over λ reduces to solving $2\lambda = \sigma(1 + \lambda^2)^2$. For small p we anticipate $\lambda \gg 1$ and hence $\lambda' = (2/\sigma)^{1/3}$ will be almost as good as the optimal λ we could find numerically. That choice leads to $p^* \leq \mu + (2^{1/3} + 2^{-2/3})\sigma^{2/3}$. For illustration, consider $\mu = 10^{-30}$ and $\sigma = 3 \times 10^{-30}$, roughly describing the small p -value estimates from the case $m_0 = m_1 = 70$. Then $p_* \leq 4 \times 10^{-20}$, much larger than μ and yet still very small. Models 1 and 2 both hold for Gaussian data Y_i . In applications, the data may be nearly Gaussian, but not exactly so, and hence there could be settings where our p^* is too small. But this numerical

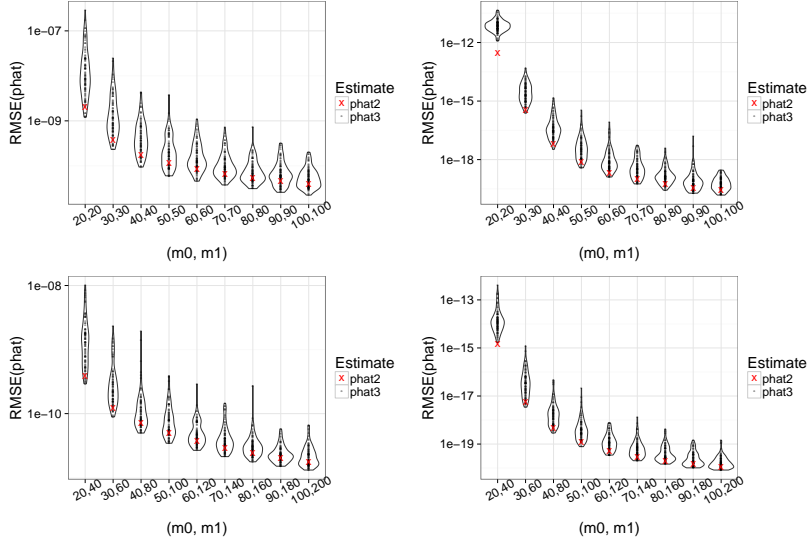


Fig 8: Comparison of $\text{RMSE}(\hat{p}_3)$ versus $\text{RMSE}(\hat{p}_2)$. The same simulation setting as described in Figure 7. The red crosses and black dots are estimated $\text{RMSE}(\hat{p}_2)$ and $\text{RMSE}(\hat{p}_3)$ under Model 2 with centers $c = 0$ and $c = \arg \max_{0 \leq i < N} |\langle \mathbf{y}_0, \mathbf{x}_i \rangle|$ respectively.

example uses a Chebychev inequality at $\lambda' \doteq 8.7 \times 10^9$ standard deviations, which ought to more than compensate for mild non-normality.

Figures 9 to 12 compare our estimates to each other and those of the saddle-point approximation, equation (1) from [Robinson \(1982\)](#). The sample sizes were $m_0 = m_1 = 10$ making it feasible to compute the exact permutation p -value for hundreds of examples. In each case we ran 500 independent simulations. Cases with perfect separation were excluded: the saddlepoint approximation is numerically unstable then, and one can easily detect that the minimum Y value in one group is larger than the maximum in the other group, showing that $p = 1/N$. Our estimates \hat{p}_2 and \hat{p}_3 are always at least as large as the granularity limit in those cases. In every instance we compared two-sided p -values.

The simulated Y_i values in group 0 come from the $t_{(5)}$, $\text{Exp}(1)$, $\mathcal{N}(0, 1)$ and $\text{U}(0, 1)$ distributions in the four figures. The Y_i values for group 1 are shifted versions of those distributions. The naive spherical cap estimator \hat{p}_1 is consistently least accurate and is often much smaller than the true p . The saddlepoint estimate is very accurate but tends to come out smaller than the true p . The improved estimators \hat{p}_2 and \hat{p}_3 are less likely to be below p than the saddlepoint estimate. We can also construct Z scores, $Z_2 = (p - \hat{p}_2)/\text{RMSE}_2$ and a similar Z_3 . If these take large values, then it means that \hat{p} is too small. The largest Z scores we observed are in Table 1. The largest Z values arose for exponential data with $p \doteq 0.89$ and $\hat{p}_2 \doteq 0.78 \doteq \hat{p}_3$. Such large p -values are not very

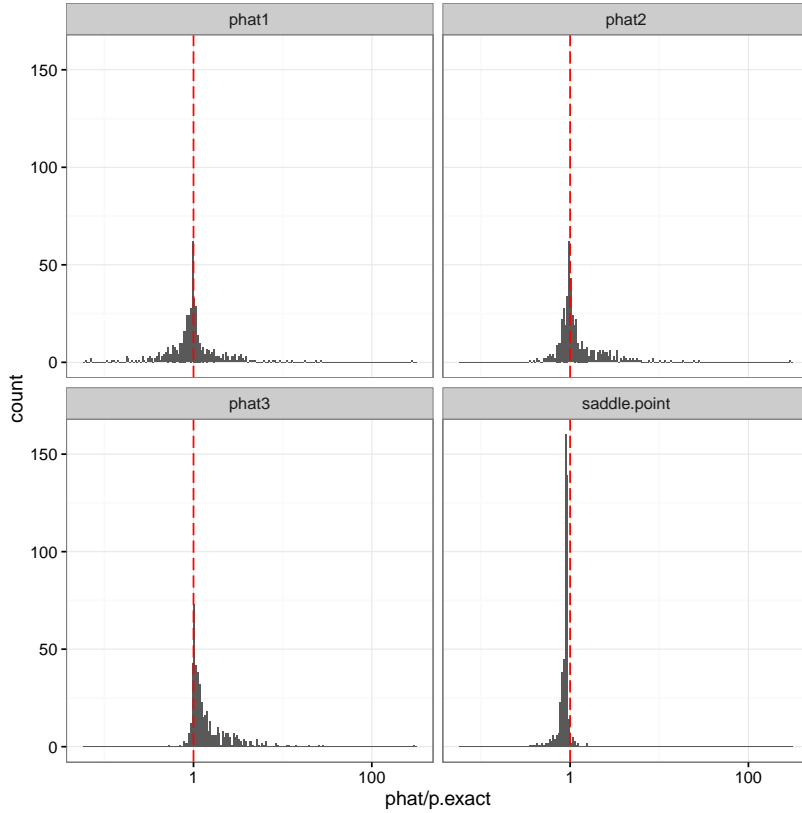


Fig 9: Simulation results \hat{p}/p as described in the text, for $Y_{0,i} \stackrel{\text{iid}}{\sim} t_{(5)}$, and $Y_{1,i} \stackrel{\text{iid}}{\sim} t_{(5)} + 1$.

important and so maximal Z scores are also shown among estimated p -values below 0.1.

9. Discussion

We have constructed approximations to the permutation p -value using probability and geometry derived from discrepancy theory. A rigorous upper bound for p could be attained using L_∞ spherical cap discrepancies instead of the L_2 version, but computing such discrepancies is a major challenge. [Narcowich et al. \(2010\)](#) give upper bounds for the L_∞ spherical cap discrepancy, in terms of averages of a great many harmonic functions at the points \mathbf{x}_i . For our application we need bounds for spherical caps of a fixed volume (under Model 1) and of fixed volume and constrained location (under Model 2) and those go beyond what is in [Narcowich et al. \(2010\)](#).

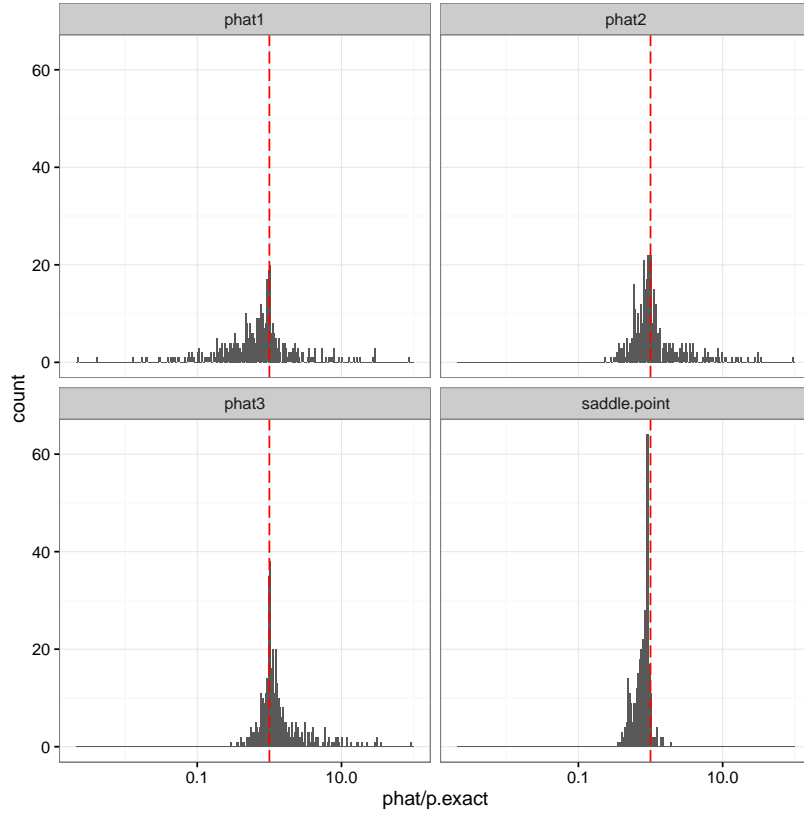


Fig 10: Simulation results \hat{p}/p as described in the text, for $Y_{0,i} \stackrel{\text{iid}}{\sim} \text{Exp}(1)$, and $Y_{1,i} \stackrel{\text{iid}}{\sim} \text{Exp}(1) + 2$.

Our motivation came from gene set testing problems, where one tests whether an ensemble of mutually correlated genes is associated with a binary variable. [Ackermann and Strimmer \(2009\)](#) make a thorough numerical comparison of 261 gene set testing methods. There were two clear winners and they were particularly simple. One summed the individual genes' t -statistics (the JG score of [Jiang and Gentleman \(2007\)](#)) over the gene set and the other summed squared t -statistics. Permutation methods were used because of correlations among the genes within a gene set. Because the simulation was focussed on coordinated small effects of several genes, the results from the JG score were virtually identical to simply correlating the binary response with the average of the genes, that is, to using a linear statistic like we study here.

To have reasonable power to obtain a p -value below ϵ by permutation sampling requires on the order of $1/\epsilon$ permutations each requiring $O(n \log(n))$ computation to generate and $O(n)$ computation to evaluate the inner product. The

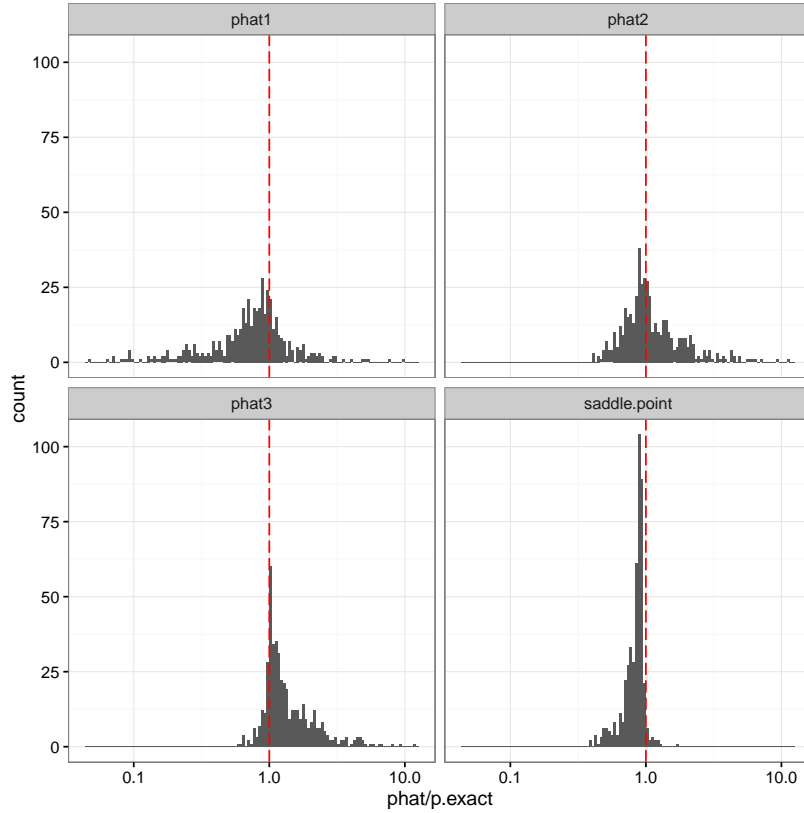


Fig 11: Simulation results \hat{p}/p as described in the text, for $Y_{0,i} \stackrel{\text{iid}}{\sim} \mathcal{N}(0, 1)$, and $Y_{1,i} \stackrel{\text{iid}}{\sim} \mathcal{N}(2, 1)$.

cost to compute the standard errors in our method is dominated by a cost proportional to \underline{m}^3 though there is a very small cost proportional to \underline{m}^4 . In the range where the first cost dominates, our proposal is advantageous when $\underline{m}^3 = o(n/\epsilon)$. Supposing that m_0 and m_1 are comparable, our advantage holds when $\underline{m}^2 = o(1/\epsilon)$. If only the estimate and not the standard error is required, then our \hat{p}_2 and \hat{p}_3 cost $O(\underline{m})$ once the \hat{p} (cost $O(n)$) has been computed. Then the total cost is $O(n)$ compared to $O(n/\epsilon)$ for sampling.

Acknowledgements

This work was supported by the US National Science Foundation under grants DMS-1407397 and DMS-1521145. We thank John Robinson for helpful comments.

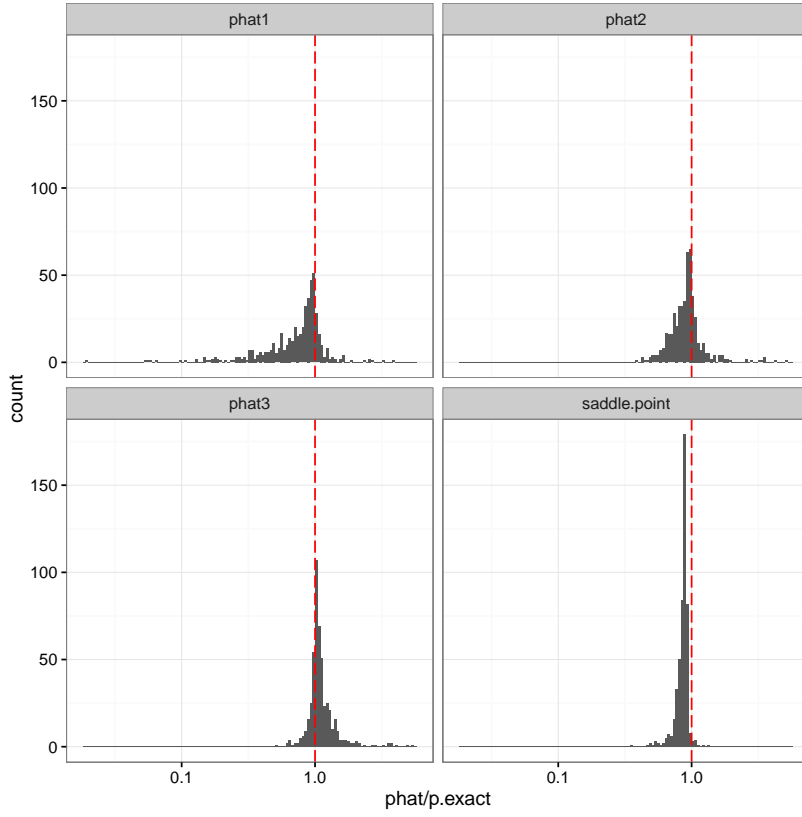


Fig 12: Simulation results \hat{p}/p as described in the text, for $Y_{0,i} \stackrel{\text{iid}}{\sim} \mathbf{U}(0, 1)$, and $Y_{1,i} \stackrel{\text{iid}}{\sim} \mathbf{U}(0, 1) + 1/2$.

References

Ackermann, M. and Strimmer, K. (2009). A general modular framework for gene set enrichment analysis. *BMC Bioinformatics*, 10:1–20.

Aronszajn, N. (1950). Theory of reproducing kernels. *Transactions of the American Mathematical Society*, 68(3):337–404.

Barnard, G. A. (1963). Discussion of the spectral analysis of point processes (by m. s. bartlett). *Journal of the Royal Statistical Society, series B*, 25:294.

Benjamini, Y. and Hochberg, Y. (1995). Controlling the false discovery rate: a practical and powerful approach to multiple testing. *Journal of the Royal Statistical Society, Series B*, pages 289–300.

Brauchart, J. and Dick, J. (2013). A simple proof of Stolarsky’s invariance principle. *Proceedings of the American Mathematical Society*, 141(6):2085–2096.

Dist'n $Y_{0,i}$	$\max Z_2$	$\max\{Z_2 \mid \hat{p}_2 < 0.1\}$	$\max Z_3$	$\max\{Z_3 \mid \hat{p}_3 < 0.1\}$
$t_{(5)}$	26.7	1.91	31.5	3.87
$\text{Exp}(1)$	7.55	7.55	7.76	7.76
$\mathbf{U}(0, 1)$	3.49	2.45	5.87	2.61
$\mathcal{N}(0, 1)$	3.07	2.78	3.07	2.78

TABLE 1
Maximal Z scores observed for \hat{p}_2 and \hat{p}_3 .

Jiang, Z. and Gentleman, R. (2007). Extensions to gene set enrichment. *Bioinformatics*, 23(3):306–313.

Knijnenburg, T. A., Wessels, L. F. A., Reinders, M. J. T., and Shmulevich, I. (2009). Fewer permutations, more accurate p-values. *Bioinformatics*, 25(12):i161–i168.

Larson, J. L. and Owen, A. B. (2015). Moment based gene set tests. *BMC Bioinformatics*, 16(1):132.

Lee, Y. and Kim, W. C. (2014). Concise formulas for the surface area of the intersection of two hyperspherical caps. Technical report, Korea advanced institute of science and technology.

Lehmann, E. L. and Romano, J. P. (2005). *Testing Statistical Hypotheses*. Springer, New York, 3rd edition.

Narcowich, F. J., Sun, X., Ward, J. D., and Wu, Z. (2010). Leveque type inequalities and discrepancy estimates for minimal energy configurations on spheres. *Journal of Approximation Theory*, 162(6):1256–1278.

Niederreiter, H. (1992). *Random Number Generation and Quasi-Monte Carlo Methods*. SIAM, Philadelphia, PA.

Reid, N. (1988). Saddlepoint methods and statistical inference. *Statistical Science*, pages 213–227.

Robinson, J. (1982). Saddlepoint approximations for permutation tests and confidence intervals. *Journal of the Royal statistical society, Series B*, pages 91–101.

Southworth, L. K., Kim, S. K., and Owen, A. B. (2009). Properties of balanced permutations. *Journal of Computational Biology*, 16(4):625–638.

Stolarsky, K. B. (1973). Sums of distances between points on a sphere. II. *Proceedings of the American Mathematical Society*, 41(2):575–582.

Zhou, C., Wang, H. J., and Wang, Y. M. (2009). Efficient moments-based permutation tests. In *Advances in neural information processing systems*, pages 2277–2285.

10. Appendix

Here we collect up some of the longer proofs.

10.1. Proof of Theorem 3 (Limiting invariance)

Here we show that taking limits as ϵ goes to zero in the formula of [Brauchart and Dick \(2013\)](#) proves Theorem 3. We use three lemmas, one for each term in Theorem 2. We use $\epsilon \rightarrow 0$ as a shorthand for $\lim_{\epsilon_1 \rightarrow 0^+} \lim_{\epsilon_2 \rightarrow 0^+}$.

Lemma 4. *Let v_ϵ be defined as in (3.3). Then for $\hat{\rho} \in [-1, 1]$,*

$$\begin{aligned} & \lim_{\epsilon \rightarrow 0} \int_{-1}^1 v_\epsilon(t) \int_{\mathbb{S}^d} \left| \sigma_d(C(\mathbf{z}; t)) - \frac{1}{N} \sum_{k=0}^{N-1} \mathbf{1}_{C(\mathbf{z}; t)}(\mathbf{x}_k) \right|^2 d\sigma_d(\mathbf{z}) dt \\ &= \int_{\mathbb{S}^d} |p(\mathbf{z}, \hat{\rho}) - \hat{p}(\hat{\rho})|^2 d\sigma_d(\mathbf{z}). \end{aligned}$$

Proof. Substituting v_ϵ we get

$$\begin{aligned} & \int_{-1}^1 \left(\epsilon_2 + \frac{1}{\epsilon_1} \mathbf{1}(\hat{\rho} \leq t \leq \hat{\rho} + \epsilon_1) \right) \int_{\mathbb{S}^d} (\hat{p}(t) - p(\mathbf{z}, t))^2 d\sigma_d(\mathbf{z}) dt \\ & \rightarrow \frac{1}{\epsilon_1} \int_{\hat{\rho}}^{\hat{\rho} + \epsilon_1} \int_{\mathbb{S}^d} (\hat{p}(t) - p(\mathbf{z}, t))^2 d\sigma_d(\mathbf{z}) dt, \quad \text{as } \epsilon_2 \rightarrow 0^+ \\ & \rightarrow \int_{\mathbb{S}^d} (\hat{p}(\hat{\rho}) - p(\mathbf{z}, \hat{\rho}))^2 d\sigma_d(\mathbf{z}), \quad \text{as } \epsilon_1 \rightarrow 0^+. \end{aligned} \quad \square$$

Lemma 5. *Let v_ϵ be as in (3.3) with $\hat{\rho} \in [-1, 1]$, and let K_{v_ϵ} be given by (3.2). Then for any $\mathbf{x}, \mathbf{x}' \in \mathbb{S}^d$,*

$$\lim_{\epsilon \rightarrow 0} K_{v_\epsilon}(\mathbf{x}, \mathbf{x}') = \sigma_d(C(\mathbf{x}; \hat{\rho}) \cap C(\mathbf{x}'; \hat{\rho})).$$

Proof. The argument is essentially the same as for Lemma 4. \square

Lemma 6. *Let v_ϵ be as in (3.3) with $\hat{\rho} \in [-1, 1]$, and let K_{v_ϵ} be given by (3.2). Then*

$$\lim_{\epsilon \rightarrow 0} \int_{\mathbb{S}^d} \int_{\mathbb{S}^d} K_{v_\epsilon}(\mathbf{x}, \mathbf{y}) d\sigma_d(\mathbf{x}) d\sigma_d(\mathbf{y}) = \hat{p}_1(\hat{\rho})^2. \quad (10.1)$$

Proof. For any $\mathbf{x}, \mathbf{y} \in \mathbb{S}^d$, the kernel $K_{v_\epsilon}(\mathbf{x}, \mathbf{y})$ is nonnegative and upper bounded by a constant. Therefore we can take our limit operations inside the double integral over \mathbf{x} and \mathbf{y} . Now $\lim_{\epsilon \rightarrow 0} K_{v_\epsilon}(\mathbf{x}, \mathbf{y}) = \int_{\mathbb{S}^d} \mathbf{1}_{C(\mathbf{z}; \hat{\rho})}(\mathbf{x}) \mathbf{1}_{C(\mathbf{z}; \hat{\rho})}(\mathbf{y}) d\sigma_d(\mathbf{z})$. Therefore the limit in (10.1) is

$$\int_{\mathbb{S}^d} \int_{\mathbb{S}^d} \int_{\mathbb{S}^d} \mathbf{1}_{C(\mathbf{z}; \hat{\rho})}(\mathbf{x}) \mathbf{1}_{C(\mathbf{z}; \hat{\rho})}(\mathbf{y}) d\sigma_d(\mathbf{z}) d\sigma_d(\mathbf{y}) d\sigma_d(\mathbf{x}) = \hat{p}_1(\hat{\rho})^2$$

after changing the order of the integrals. \square

Theorem 3 *Let $\mathbf{x}_0, \mathbf{x}_1, \dots, \mathbf{x}_N \in \mathbb{S}^d$ and $\hat{\rho} \in [-1, 1]$. Then*

$$\int_{\mathbb{S}^d} |p(\mathbf{z}, \hat{\rho}) - \hat{p}_1(\hat{\rho})|^2 d\sigma_d(\mathbf{z}) = \frac{1}{N^2} \sum_{k=0}^{N-1} \sum_{l=0}^{N-1} \sigma_d(C(\mathbf{x}_k; \hat{\rho}) \cap C(\mathbf{x}_l; \hat{\rho})) - \hat{p}_1(\hat{\rho})^2.$$

Proof. Theorem 2 gives us an identity and applying Lemmas 4, 5 and 6 to both sides of it establishes (3.4) for $\rho \in [-1, 1]$. For $\hat{\rho} = 1$ we get the answer by replacing v_ϵ by $\epsilon_2 + (1/\epsilon_1)\mathbf{1}_{1-\epsilon_1 \leq t \leq 1}$ in the lemmas. Replacing \mathbf{z} by \mathbf{y} and $\hat{\rho}$ by t above gives the version in the main body of the article. \square

10.2. Proof of Lemma 3 (Double inclusion for Model 2)

Proof. We split the proof into four cases and prove them individually. Recall that $P_2(u_1, u_2, u_3, \tilde{\rho}, \hat{\rho}) = \int_{\mathbb{S}^{d-1}} \mathbf{1}(\langle \mathbf{y}, \mathbf{x}_1 \rangle \geq \hat{\rho}) \mathbf{1}(\langle \mathbf{y}, \mathbf{x}_2 \rangle \geq \hat{\rho}) d\sigma_{d-1}(\mathbf{y}^*)$ where $\mathbf{y} = \tilde{\rho} \mathbf{x}_c + \sqrt{1 - \tilde{\rho}^2} \mathbf{y}^*$.

Case 1. $\mathbf{x}_1 = \mathbf{x}_2 = \mathbf{x}_c$, i.e., $r_1 = r_2 = r_3 = 0$.

$$P_2(1, 1, 1, \tilde{\rho}, \hat{\rho}) = \int_{\mathbb{S}^{d-1}} \mathbf{1}(\langle \mathbf{y}, \mathbf{x}_c \rangle \geq \hat{\rho}) \mathbf{1}(\langle \mathbf{y}, \mathbf{x}_c \rangle \geq \hat{\rho}) d\sigma_{d-1}(\mathbf{y}^*) = \mathbf{1}(\tilde{\rho} \geq \hat{\rho}).$$

Case 2. $\mathbf{x}_1 = \mathbf{x}_c \neq \mathbf{x}_2$, i.e., $r_1 = 0, r_2 > 0, r_3 > 0$.

$$\begin{aligned} P_2(1, u_2, u_2, \tilde{\rho}, \hat{\rho}) &= \int_{\mathbb{S}^{d-1}} \mathbf{1}(\langle \mathbf{y}, \mathbf{x}_c \rangle \geq \hat{\rho}) \mathbf{1}(\langle \mathbf{y}, \mathbf{x}_2 \rangle \geq \hat{\rho}) d\sigma_{d-1}(\mathbf{y}^*) \\ &= \mathbf{1}(\tilde{\rho} \geq \hat{\rho}) \int_{\mathbb{S}^{d-1}} \mathbf{1}(\langle \mathbf{y}, \mathbf{x}_2 \rangle \geq \hat{\rho}) d\sigma_{d-1}(\mathbf{y}^*) \\ &= \mathbf{1}(\tilde{\rho} \geq \hat{\rho}) P_1(u_2, \tilde{\rho}, \hat{\rho}) \end{aligned}$$

where the last step uses Lemma 2.

Case 3. $\mathbf{x}_1 = \mathbf{x}_2 \neq \mathbf{x}_c$, i.e., $r_1 = r_2 > 0 = r_3$.

$$\begin{aligned} P_2(u_2, u_2, 1, \tilde{\rho}, \hat{\rho}) &= \int_{\mathbb{S}^{d-1}} \mathbf{1}(\langle \mathbf{y}, \mathbf{x}_1 \rangle \geq \hat{\rho}) \mathbf{1}(\langle \mathbf{y}, \mathbf{x}_2 \rangle \geq \hat{\rho}) d\sigma_{d-1}(\mathbf{y}^*) \\ &= \int_{\mathbb{S}^{d-1}} \mathbf{1}(\langle \mathbf{y}, \mathbf{x}_2 \rangle \geq \hat{\rho}) d\sigma_{d-1}(\mathbf{y}^*) \\ &= P_1(u_2, \tilde{\rho}, \hat{\rho}). \end{aligned}$$

Case 4. $\mathbf{x}_1 \neq \mathbf{x}_2 \neq \mathbf{x}_c \neq \mathbf{x}_1$, i.e., $r_1, r_2, r_3 > 0$. We split this case into subcases. First we assume $u_2 = -1$, so

$$\begin{aligned} P_2(u_1, u_2, u_3, \tilde{\rho}, \hat{\rho}) &= \int_{\mathbb{S}^{d-1}} \mathbf{1}(\langle \mathbf{y}, \mathbf{x}_1 \rangle \geq \hat{\rho}) \mathbf{1}(\langle \mathbf{y}, -\mathbf{x}_c \rangle \geq \hat{\rho}) d\sigma_{d-1}(\mathbf{y}^*) \\ &= \mathbf{1}(-\tilde{\rho} \geq \hat{\rho}) \int_{\mathbb{S}^{d-1}} \mathbf{1}(\langle \mathbf{y}, \mathbf{x}_1 \rangle \geq \hat{\rho}) d\sigma_{d-1}(\mathbf{y}^*) \\ &= \mathbf{1}(-\tilde{\rho} \geq \hat{\rho}) P_1(u_1, \tilde{\rho}, \hat{\rho}). \end{aligned}$$

Similarly if $u_1 = -1$, then

$$P_2(u_1, u_2, u_3, \tilde{\rho}, \hat{\rho}) = \mathbf{1}(-\tilde{\rho} \geq \hat{\rho}) P_1(u_2, \tilde{\rho}, \hat{\rho}).$$

Finally we assume $u_1 > -1$ and $u_2 > -1$, so now $|u_1| < 1$ and $|u_2| < 1$. Recall the projections $\mathbf{x}_j = u_j \mathbf{c}_c + \sqrt{1 - u_j^2} \mathbf{x}_j^*$ for $j = 1, 2$ and introduce

further projections of \mathbf{y}^* and \mathbf{x}_2^* onto \mathbf{x}_1^* : $\mathbf{y}^* = t\mathbf{x}_1^* + \sqrt{1-t^2}\mathbf{y}^{**}$ and $\mathbf{x}_2^* = u_3^*\mathbf{x}_1^* + \sqrt{1-u_3^{*2}}\mathbf{x}_2^{**}$. The residuals \mathbf{y}^{**} and \mathbf{x}_2^{**} belong to a subset of \mathbb{S}^d that is isomorphic to \mathbb{S}^{d-2} . Now we have

$$\begin{aligned}
P_2(u_1, u_2, u_3, \tilde{\rho}, \hat{\rho}) &= \int_{\mathbb{S}^{d-1}} \mathbf{1}(\langle \mathbf{y}, \mathbf{x}_1 \rangle \geq \hat{\rho}) \mathbf{1}(\langle \mathbf{y}, \mathbf{x}_2 \rangle \geq \hat{\rho}) d\sigma_{d-1}(\mathbf{y}^*) \\
&= \int_{-1}^1 \frac{\omega_{d-2}}{\omega_{d-1}} (1-t^2)^{\frac{d-1}{2}-1} \int_{\mathbb{S}^{d-2}} \mathbf{1}(\tilde{\rho}u_1 + \sqrt{1-\tilde{\rho}^2}\sqrt{1-u_1^2}t \geq \hat{\rho}) \\
&\quad \times \mathbf{1}(\tilde{\rho}u_2 + \sqrt{1-\tilde{\rho}^2}\sqrt{1-u_2^2}(tu_3^* + \sqrt{1-t^2}\sqrt{1-u_3^{*2}}\langle \mathbf{y}^{**}, \mathbf{x}_2^{**} \rangle) \geq \hat{\rho}) \\
&\quad \times d\sigma_{d-1}(\mathbf{y}^{**}) dt \\
&= \int_{-1}^1 \frac{\omega_{d-2}}{\omega_{d-1}} (1-t^2)^{\frac{d-1}{2}-1} \mathbf{1}\left(t \geq \frac{\hat{\rho} - \tilde{\rho}u_1}{\sqrt{1-\tilde{\rho}^2}\sqrt{1-u_1^2}}\right) \\
&\quad \times \int_{\mathbb{S}^{d-2}} \mathbf{1}(\tilde{\rho}u_2 + \sqrt{1-\tilde{\rho}^2}\sqrt{1-u_2^2}(tu_3^* + \sqrt{1-t^2}\sqrt{1-u_3^{*2}}\langle \mathbf{y}^{**}, \mathbf{x}_2^{**} \rangle) \geq \hat{\rho}) \\
&\quad \times d\sigma_{d-1}(\mathbf{y}^{**}) dt \\
&= \begin{cases} \mathbf{1}(\tilde{\rho}u_1 \geq \hat{\rho}) \mathbf{1}(\tilde{\rho}u_2 \geq \hat{\rho}), & \tilde{\rho} = \pm 1 \\ \int_{-1}^1 \frac{\omega_{d-2}}{\omega_{d-1}} (1-t^2)^{\frac{d-1}{2}-1} \mathbf{1}(t \geq \rho_1) \mathbf{1}(tu_3^* \geq \rho_2) dt, & \tilde{\rho} \neq \pm 1, u_3^* = \pm 1 \\ \int_{-1}^1 \frac{\omega_{d-2}}{\omega_{d-1}} (1-t^2)^{\frac{d-1}{2}-1} \mathbf{1}(t \geq \rho_1) \sigma_{d-2}(C(\mathbf{x}_2^{**}, \frac{\rho_2 - tu_3^*}{\sqrt{1-t^2}\sqrt{1-u_3^{*2}}})) dt, & \tilde{\rho} \neq \pm 1, |u_3^*| < 1 \end{cases}
\end{aligned}$$

where u_3^*, ρ_1, ρ_2 are defined in (4.7). Hence, the result follows. \square

10.3. Proof of Theorem 6 (Second moment under Model 2)

Proof. Without loss of generality we relabel the values \mathbf{x}_k so that $c = 0$. Any other choice for c is reflected in the number $\tilde{\rho}$. The second moment is

$$\mathbb{E}(p(\mathbf{y}, \hat{\rho})^2) = \frac{1}{N^2} \sum_{k=0}^{N-1} \sum_{l=0}^{N-1} P_2(u_k, u_l, u_{k,l}, \tilde{\rho}, \hat{\rho}) \quad (10.2)$$

where $r_{k,l}$ is the swap distance between points \mathbf{x}_k and \mathbf{x}_l . We will partition the sum in (10.2) into the same four cases as in the proof of Lemma 3.

Case 1, $\mathbf{x}_k = \mathbf{x}_l = \mathbf{x}_c$, i.e., $r_k = r_l = r_{k,l} = 0$. There is only one pair of $(\mathbf{x}_k, \mathbf{x}_l)$ for this condition. Hence, we get only one term corresponding to $P_2(1, 1, 1, \tilde{\rho}, \hat{\rho}) = \mathbf{1}(\tilde{\rho} \geq \hat{\rho})$.

Case 2, $\mathbf{x}_k = \mathbf{x}_c \neq \mathbf{x}_l$, i.e., $r_k = 0, r_l = r_{k,l} > 0$. Consider all pairs of $(\mathbf{x}_k, \mathbf{x}_l)$ that satisfy this condition and let K_2 denote their total contribution to (10.2).

Then

$$\begin{aligned} K_2 &= 2 \sum_{l=1}^{N-1} \int_{\mathbb{S}^{d-1}} \mathbf{1}(\langle \mathbf{y}, \mathbf{x}_c \rangle \geq \hat{\rho}) \mathbf{1}(\langle \mathbf{y}, \mathbf{x}_l \rangle \geq \hat{\rho}) d\sigma_{d-1}(\mathbf{y}^*) \\ &= 2 \sum_{r=1}^{\frac{m}{2}} \binom{m_0}{r} \binom{m_1}{r} P_2(1, u(r), u(r), \tilde{\rho}, \hat{\rho}). \end{aligned}$$

Case 3, $\mathbf{x}_k = \mathbf{x}_l \neq \mathbf{x}_c$, i.e., $r_k = r_l > 0 = r_{k,l}$. The contribution from terms of this form is

$$K_3 = \sum_{k=1}^{N-1} \int_{\mathbb{S}^{d-1}} \mathbf{1}(\langle \mathbf{y}, \mathbf{x}_k \rangle \geq \hat{\rho}) d\sigma_{d-1}(\mathbf{y}^*) = \sum_{r=1}^{\frac{m}{2}} \binom{m_0}{r} \binom{m_1}{r} P_1(u(r), \tilde{\rho}, \hat{\rho}).$$

Case 4, $\mathbf{x}_k \neq \mathbf{x}_l \neq \mathbf{x}_c$, i.e., $r_k, r_l, r_{k,l} > 0$. The contribution of these cases to the sum is

$$\begin{aligned} K_4 &= \sum_{k=1}^{N-1} \sum_{l=1}^{N-1} \mathbf{1}(l \neq k) \int_{\mathbb{S}^{d-1}} \mathbf{1}(\langle \mathbf{y}, \mathbf{x}_i \rangle \geq \hat{\rho}) \mathbf{1}(\langle \mathbf{y}, \mathbf{x}_j \rangle \geq \hat{\rho}) d\sigma_{d-1}(\mathbf{y}^*) \\ &= \sum_{r_k \in R} \sum_{r_l \in R} \sum_{r_{k,l} \in R_3(\mathbf{r})} c(r_k, r_l, r_{k,l}) P_2(u_1, u_2, u_3, \tilde{\rho}, \hat{\rho}). \end{aligned}$$

Then the second moment is $(\mathbf{1}(\tilde{\rho} \geq \hat{\rho}) + K_2 + K_3 + K_4)/N^2$. \square

10.4. Proof of Theorem 7 (Location weighted invariance)

Proof. We follow the technique in [Brauchart and Dick \(2013\)](#). We begin by showing that $K_{v,h,\mathbf{x}'}$ as defined in (5.2) is a reproducing kernel. First, $K_{v,h,\mathbf{x}'}$ is symmetric: $K_{v,h,\mathbf{x}'}(\mathbf{x}, \mathbf{y}) = K_{v,h,\mathbf{x}'}(\mathbf{y}, \mathbf{x})$. Next, choose $a_0, \dots, a_{N-1} \in \mathbb{R}$ and $\mathbf{x}_0, \dots, \mathbf{x}_{N-1} \in \mathbb{S}^d$. Then $\sum_{k,l=0}^{N-1} a_k a_l K_{v,h,\mathbf{x}'}(\mathbf{x}_k, \mathbf{x}_l)$ equals

$$\begin{aligned} &\int_{-1}^1 \int_{\mathbb{S}^d} \sum_{k,l=0}^{N-1} a_k a_l v(t) h(\langle \mathbf{z}, \mathbf{x}' \rangle) \mathbf{1}_{C(\mathbf{z};t)}(\mathbf{x}_k) \mathbf{1}_{C(\mathbf{z};t)}(\mathbf{x}_l) d\sigma_d(\mathbf{z}) dt \\ &= \int_{-1}^1 \int_{\mathbb{S}^d} v(t) h(\langle \mathbf{z}, \mathbf{x}' \rangle) \left| \sum_{k=0}^{N-1} a_k \mathbf{1}_{C(\mathbf{z},t)}(\mathbf{x}_k) \right|^2 d\sigma_d(\mathbf{z}) dt \end{aligned}$$

which is nonnegative. Thus $K_{v,h,\mathbf{x}'}$ is symmetric and positive definite, and so by [Aronszajn \(1950\)](#), $K_{v,h,\mathbf{x}'}$ is a reproducing kernel.

[Aronszajn \(1950\)](#) also shows that a reproducing kernel uniquely defines a Hilbert space of functions with a specific inner product. Let $\mathcal{H}_{v,h,\mathbf{x}'} = \mathcal{H}(K_{v,h,\mathbf{x}'}, \mathbb{S}^d)$ denote the corresponding reproducing kernel Hilbert space of functions $f : \mathbb{S}^d \rightarrow \mathbb{R}$ with reproducing kernel $K_{v,h,\mathbf{x}'}$.

We now consider functions $f_1, f_2 : \mathbb{S}^d \rightarrow \mathbb{R}$ which admit the representation

$$f_i(\mathbf{x}) = \int_{-1}^1 \int_{\mathbb{S}^d} g_i(\mathbf{z}; t) \mathbf{1}_{C(\mathbf{z}; t)}(\mathbf{x}) d\sigma_d(\mathbf{z}) dt, \quad i = 1, 2 \quad (10.3)$$

for functions $g_i \in L_2(\mathbb{S}^d \times [-1, 1])$. For any fixed $\mathbf{y} \in \mathbb{S}^d$ the function $K_{v, h, \mathbf{x}'}(\cdot, \mathbf{y})$ has representation (10.3) via $g(\mathbf{z}; t) = v(t)h(\langle \mathbf{z}, \mathbf{x}' \rangle) \mathbf{1}_{C(\mathbf{z}, t)}(\mathbf{y})$.

For functions with representation (10.3), we define an inner product by

$$\langle f_1, f_2 \rangle_{K_{v, h, \mathbf{x}'}} = \int_{-1}^1 \frac{1}{v(t)} \int_{\mathbb{S}^d} \frac{1}{h(\langle \mathbf{z}, \mathbf{x}' \rangle)} g_1(\mathbf{z}, t) g_2(\mathbf{z}, t) d\sigma_d(\mathbf{z}) dt. \quad (10.4)$$

For $\mathbf{y} \in \mathbb{S}^d$ and $f_1 \in \mathcal{H}_{v, h, \mathbf{x}'}$,

$$\begin{aligned} \langle f_1, K_{v, h, \mathbf{x}'}(\cdot, \mathbf{y}) \rangle_{K_{v, h, \mathbf{x}'}} &= \int_{-1}^1 \frac{1}{v(t)} \int_{\mathbb{S}^d} \frac{g_1(\mathbf{z}; t) v(t)}{h(\langle \mathbf{z}, \mathbf{x}' \rangle)} h(\langle \mathbf{z}, \mathbf{x}' \rangle) \mathbf{1}_{C(\mathbf{z}; t)}(\mathbf{y}) d\sigma_d(\mathbf{z}) dt \\ &= \int_{-1}^1 \int_{\mathbb{S}^d} g_1(\mathbf{z}, t) \mathbf{1}_{C(\mathbf{z}, t)}(\mathbf{y}) d\sigma_d(\mathbf{z}) dt \\ &= f_1(\mathbf{y}), \end{aligned}$$

showing that the inner product (10.4) has the reproducing property. By [Aronszajn \(1950\)](#), the inner product in $\mathcal{H}_{v, h, \mathbf{x}'}$ is unique. Functions f_i satisfying (10.3) with $\langle f_i, f_i \rangle_{K_{v, h, \mathbf{x}'}} < \infty$ are in $\mathcal{H}_{v, h, \mathbf{x}'}$, and (10.4) is the unique inner product of $\mathcal{H}_{v, h, \mathbf{x}'}$.

We prove the theorem by equating two different forms of $\|\mathcal{R}(\mathcal{H}_{v, h, \mathbf{x}'}; \cdot)\|_{K_{v, h, \mathbf{x}'}}$ where

$$\mathcal{R}(\mathcal{H}_{v, h, \mathbf{x}'}; \cdot) = \int_{\mathbb{S}^d} K_{v, h, \mathbf{x}'}(\cdot, \mathbf{y}) d\sigma_d(\mathbf{y}) - \frac{1}{N} \sum_{k=0}^{N-1} K_{v, h, \mathbf{x}'}(\cdot, \mathbf{x}_k).$$

Although $\mathcal{R}(\mathcal{H}_{v, h, \mathbf{x}'}; \cdot)$ depends on our specific points \mathbf{x}_i we omit that from the notation. The reproducing property of $K_{v, h, \mathbf{x}'}$ yields

$$\langle K_{v, h, \mathbf{x}'}(\cdot, \mathbf{x}_k), K_{v, h, \mathbf{x}'}(\cdot, \mathbf{x}_l) \rangle_{K_{v, h, \mathbf{x}'}} = K_{v, h, \mathbf{x}'}(\mathbf{x}_k, \mathbf{x}_l)$$

from which it follows that

$$\begin{aligned} &\left\langle \int_{\mathbb{S}^d} K_{v, h, \mathbf{x}'}(\cdot, \mathbf{y}) d\sigma_d(\mathbf{y}), \int_{\mathbb{S}^d} K_{v, h, \mathbf{x}'}(\cdot, \mathbf{y}') d\sigma_d(\mathbf{y}') \right\rangle_{K_{v, h, \mathbf{x}'}} \\ &= \int_{\mathbb{S}^d} \int_{\mathbb{S}^d} K_{v, h, \mathbf{x}'}(\mathbf{y}, \mathbf{y}') d\sigma_d(\mathbf{y}) d\sigma_d(\mathbf{y}'). \end{aligned} \quad (10.5)$$

Using (10.5) and the linearity of the inner product, we have

$$\begin{aligned}
& \langle \mathcal{R}(\mathcal{H}_{v,h,\mathbf{x}'}; \cdot), \mathcal{R}(\mathcal{H}_{v,h,\mathbf{x}'}; \cdot) \rangle_{K_{v,h,\mathbf{x}'}} \\
&= \int_{\mathbb{S}^d} \int_{\mathbb{S}^d} K_{v,h,\mathbf{x}'}(\mathbf{y}, \mathbf{y}') d\sigma_d(\mathbf{y}) d\sigma_d(\mathbf{y}') - \frac{2}{N} \sum_{k=0}^{N-1} \int_{\mathbb{S}^d} K_{v,h,\mathbf{x}'}(\mathbf{y}, \mathbf{x}_k) d\sigma_d(\mathbf{y}) \\
&\quad + \frac{1}{N^2} \sum_{k,l=0}^{N-1} K_{v,h,\mathbf{x}'}(\mathbf{x}_k, \mathbf{x}_l).
\end{aligned} \tag{10.6}$$

For our second form of $\|\mathcal{R}(\mathcal{H}_{v,h,\mathbf{x}'}; \cdot)\|_{K_{v,h,\mathbf{x}'}}$, we write

$$\begin{aligned}
& \mathcal{R}(\mathcal{H}_{v,h,\mathbf{x}'}; \cdot) \\
&= \int_{\mathbb{S}^d} K_{v,h,\mathbf{x}'}(\cdot, \mathbf{y}) d\sigma_d(\mathbf{y}) - \frac{1}{N} \sum_{k=0}^{N-1} K_{v,h,\mathbf{x}'}(\cdot, \mathbf{x}_k) \\
&= \int_{-1}^1 v(t) \int_{\mathbb{S}^d} \mathbf{1}_{C(\mathbf{z};t)}(\mathbf{x}) h(\langle \mathbf{z}, \mathbf{x} \rangle) \left[\int_{\mathbb{S}^d} \mathbf{1}_{C(\mathbf{z},t)}(\mathbf{y}) d\sigma_d(\mathbf{y}) dt - \frac{1}{N} \sum_{k=0}^{N-1} \mathbf{1}_{C(\mathbf{z},t)}(\mathbf{x}_k) \right] d\sigma_d(\mathbf{z}) dt \\
&= \int_{-1}^1 v(t) \int_{\mathbb{S}^d} \mathbf{1}_{C(\mathbf{z},t)}(\mathbf{x}) h(\langle \mathbf{z}, \mathbf{x} \rangle) \left[\sigma_d(C(\mathbf{z},t)) - \frac{1}{N} \sum_{k=0}^{N-1} \mathbf{1}_{C(\mathbf{z},t)}(\mathbf{x}_k) \right] d\sigma_d(\mathbf{z}) dt.
\end{aligned}$$

Hence using the definition of the inner product $\langle \cdot, \cdot \rangle_{K_{v,h,\mathbf{x}'}}$, we have

$$\begin{aligned}
& \langle \mathcal{R}(\mathcal{H}_{v,h,\mathbf{x}'}; \mathbf{x}), \mathcal{R}(\mathcal{H}_{v,h,\mathbf{x}'}; \mathbf{x}) \rangle_{K_{v,h,\mathbf{x}'}} \\
&= \int_{-1}^1 v(t) \int_{\mathbb{S}^d} h(\langle \mathbf{z}, \mathbf{x} \rangle) \left| \sigma_d(C(\mathbf{x},t)) - \frac{1}{N} \sum_{k=0}^{N-1} \mathbf{1}_{C(\mathbf{x},t)}(\mathbf{x}_k) \right|^2 d\sigma_d(\mathbf{x}) dt.
\end{aligned} \tag{10.7}$$

Combining equations (10.6) and (10.7), we have the generalized location-weighted version of the Stolarsky invariance principle. \square

10.5. Proof of Theorem 8 (Spatially weighed invariance)

As in Section 10.1, $\lim_{\epsilon \rightarrow 0}$ means $\lim_{\epsilon_1 \rightarrow 0^+} \lim_{\epsilon_2 \rightarrow 0^+}$ and similarly $\lim_{\eta \rightarrow 0}$ denotes $\lim_{\eta_1 \rightarrow 0^+} \lim_{\eta_2 \rightarrow 0^+}$. We prove a series of lemmas first.

Lemma 7. For $v_\epsilon(\cdot)$ and $h_\eta(\cdot)$ defined by equations (3.3) and (5.3),

$$\begin{aligned}
& \lim_{\eta \rightarrow 0} \lim_{\epsilon \rightarrow 0} \int_{-1}^1 v_\epsilon(t) \int_{\mathbb{S}^d} h_\eta(\langle \mathbf{z}, \mathbf{x}_c \rangle) \left| \sigma_d(C(\mathbf{z},t)) - \frac{1}{N} \sum_{k=0}^{N-1} \mathbf{1}_{C(\mathbf{z},t)}(\mathbf{x}_k) \right|^2 d\sigma_d(\mathbf{z}) dt \\
&= \int_{\mathbb{S}^{d-1}} |p(\tilde{\rho} \mathbf{x}_c + \sqrt{1 - \tilde{\rho}^2} \mathbf{y}^*, \hat{\rho}) - \hat{p}_1(\hat{\rho})|^2 d\sigma_{d-1}(\mathbf{y}^*),
\end{aligned}$$

where $\hat{p}_1(\hat{\rho}) = \sigma_d(C(\mathbf{y}; \hat{\rho}))$.

Proof. This proof is similar to the others. First we take the limit $\epsilon \rightarrow 0$ yielding

$$\lim_{\eta \rightarrow 0} \int_{\mathbb{S}^d} h_{\eta}(\langle \mathbf{z}, \mathbf{x}_c \rangle) \left| \sigma_d(C(\mathbf{z}, \hat{\rho})) - \frac{1}{N} \sum_{k=1}^N \mathbf{1}_{C(\mathbf{z}; \hat{\rho})}(\mathbf{x}_k) \right|^2 d\sigma_d(\mathbf{z}).$$

Making the projection $\mathbf{z} = s\mathbf{x}_c + \sqrt{1-s^2}\mathbf{z}^*$ gives

$$\begin{aligned} & \lim_{\eta \rightarrow 0} \int_{-1}^1 \int_{\mathbb{S}^{d-1}} \frac{\omega_{d-1}}{\omega_d} (1-s^2)^{d/2-1} h_{\eta}(s) \times \\ & \quad \left| \sigma_d(C(s\mathbf{x}_c + \sqrt{1-s^2}\mathbf{z}^*, \hat{\rho})) - \frac{1}{N} \sum_{k=1}^N \mathbf{1}_{C(s\mathbf{x}_c + \sqrt{1-s^2}\mathbf{z}^*; \hat{\rho})}(\mathbf{x}_k) \right|^2 d\sigma_{d-1}(\mathbf{z}^*) ds \\ & = \int_{\mathbb{S}^{d-1}} |p(\hat{\rho}\mathbf{x}_c + \sqrt{1-\hat{\rho}^2}\mathbf{y}^*, \hat{\rho}) - \hat{p}_1(\hat{\rho})|^2 d\sigma_{d-1}(\mathbf{y}^*). \end{aligned} \quad \square$$

Lemma 8. For $v_{\epsilon}(\cdot)$ and $h_{\eta}(\cdot)$ defined by equations (3.3) and (5.3) ,

$$\begin{aligned} & \lim_{\eta \rightarrow 0} \lim_{\epsilon \rightarrow 0} \frac{1}{N^2} \sum_{k,l=0}^{N-1} K_{v_{\epsilon}, h_{\eta}, \mathbf{x}_c}(\mathbf{x}_k, \mathbf{x}_l) \\ & = \frac{1}{N^2} \sum_{k,l=0}^{N-1} \int_{\mathbb{S}^{d-1}} \mathbf{1}(\langle \mathbf{y}, \mathbf{x}_k \rangle \geq \hat{\rho}) \mathbf{1}(\langle \mathbf{y}, \mathbf{x}_l \rangle \geq \hat{\rho}) d\sigma_{d-1}(\mathbf{y}^*). \end{aligned}$$

Proof. First, $\lim_{\eta \rightarrow 0} \lim_{\epsilon \rightarrow 0} N^{-2} \sum_{k,l=0}^{N-1} K_{v_{\epsilon}, h_{\eta}, \mathbf{x}_c}(\mathbf{x}_k, \mathbf{x}_l)$ equals

$$\frac{1}{N^2} \sum_{k,l=0}^{N-1} \lim_{\eta \rightarrow 0} \int_{\mathbb{S}^d} h_{\eta}(\langle \mathbf{z}, \mathbf{x}_c \rangle) \mathbf{1}_{C(\mathbf{z}; \hat{\rho})}(\mathbf{x}_k) \mathbf{1}_{C(\mathbf{z}; \hat{\rho})}(\mathbf{x}_l) d\sigma_d(\mathbf{z}).$$

Projecting \mathbf{z} onto \mathbf{x}_c yields $\mathbf{z} = s\mathbf{x}_c + \sqrt{1-s^2}\mathbf{y}^*$ and then we have

$$\begin{aligned} & \frac{1}{N^2} \sum_{k,l=0}^{N-1} \lim_{\eta \rightarrow 0} \int_{-1}^1 \frac{\omega_{d-1}}{\omega_d} (1-s^2)^{d/2-1} h_{\eta}(s) \int_{\mathbb{S}^{d-1}} \mathbf{1}_{C(\mathbf{z}; \hat{\rho})}(\mathbf{x}_k) \mathbf{1}_{C(\mathbf{z}; \hat{\rho})}(\mathbf{x}_l) d\sigma_{d-1}(\mathbf{y}^*) \\ & = \frac{1}{N^2} \sum_{k,l=0}^{N-1} \int_{\mathbb{S}^{d-1}} \mathbf{1}(\langle \mathbf{y}, \mathbf{x}_k \rangle \geq \hat{\rho}) \mathbf{1}(\langle \mathbf{y}, \mathbf{x}_l \rangle \geq \hat{\rho}) d\sigma_{d-1}(\mathbf{y}^*). \end{aligned} \quad \square$$

Lemma 9. For $v_{\epsilon}(\cdot)$ and $h_{\eta}(\cdot)$ defined by equations (3.3) and (5.3),

$$\lim_{\eta \rightarrow 0} \lim_{\epsilon \rightarrow 0} \int_{\mathbb{S}^d} \int_{\mathbb{S}^d} K_{v_{\epsilon}, h_{\eta}, \mathbf{x}_c}(\mathbf{x}, \mathbf{y}) d\sigma_d(\mathbf{x}) d\sigma_d(\mathbf{y}) = \hat{p}_1(\hat{\rho})^2$$

Proof. Because $K_{v_{\epsilon}, h_{\eta}, \mathbf{x}_c}$ is nonnegative and uniformly bounded we may take the limit over ϵ inside the integrals. Now

$$\lim_{\epsilon \rightarrow 0} K_{v_{\epsilon}, h_{\eta}, \mathbf{x}_c}(\mathbf{x}, \mathbf{y}) = \int_{\mathbb{S}^d} h_{\eta}(\langle \mathbf{z}, \mathbf{x}_c \rangle) \mathbf{1}_{C(\mathbf{z}; \hat{\rho})}(\mathbf{x}) \mathbf{1}_{C(\mathbf{z}; \hat{\rho})}(\mathbf{y}) d\sigma_d(\mathbf{z}),$$

and the limit becomes

$$\lim_{\eta \rightarrow 0} \int_{\mathbb{S}^d} \int_{\mathbb{S}^d} \int_{\mathbb{S}^d} h_{\eta}(\langle \mathbf{z}, \mathbf{x}_c \rangle) \mathbf{1}_{C(\mathbf{z}; \hat{\rho})}(\mathbf{x}) \mathbf{1}_{C(\mathbf{z}; \hat{\rho})}(\mathbf{y}) d\sigma_d(\mathbf{z}) d\sigma_d(\mathbf{x}) d\sigma_d(\mathbf{y}).$$

Integrating over \mathbf{z} last we get $\lim_{\eta \rightarrow 0} \int_{\mathbb{S}^d} h_{\eta}(\langle \mathbf{z}, \mathbf{x}_c \rangle) \hat{p}_1^2(\hat{\rho}) d\mathbf{z} = \hat{p}_1^2(\hat{\rho})$. \square

Lemma 10. *Under Model 2*

$$\lim_{\eta \rightarrow 0} \lim_{\epsilon \rightarrow 0} \frac{2}{N} \sum_{k=0}^{N-1} \int_{\mathbb{S}^d} K_{v_{\epsilon}, h_{\eta}, \mathbf{x}_c}(\mathbf{x}, \mathbf{x}_k) d\sigma_d(\mathbf{x}) = 2\hat{p}_1(\hat{\rho}) \mathbb{E}(p(\mathbf{y}, \hat{\rho})).$$

Proof. The argument here is similar to the one used for Lemma 9. Take the limit over ϵ inside the integral and change the order of integration to yield

$$\lim_{\eta \rightarrow 0} 2\hat{p}_1(\hat{\rho}) \int_{\mathbb{S}^d} \frac{1}{N} \sum_{k=0}^{N-1} h_{\eta}(\langle \mathbf{z}, \mathbf{x}_c \rangle) \mathbf{1}_{C(\mathbf{z}, \hat{\rho})}(\mathbf{x}_k) d\sigma_d(\mathbf{z}).$$

Substituting the projection $\mathbf{z} = t\mathbf{x}_c + \sqrt{1-t^2}\mathbf{z}^*$ produces

$$\begin{aligned} & \lim_{\eta \rightarrow 0} 2\hat{p}_1(\hat{\rho}) \int_{-1}^1 \frac{\omega_{d-1}}{\omega_d} (1-t^2)^{d/2-1} h_{\eta}(t) \int_{\mathbb{S}^{d-1}} \frac{1}{N} \sum_{k=0}^{N-1} \mathbf{1}_{C(t\mathbf{x}_c + \sqrt{1-t^2}\mathbf{z}^*, \hat{\rho})}(\mathbf{x}_k) d\sigma_{d-1}(\mathbf{z}^*) dt \\ &= 2\hat{p}_1(\hat{\rho}) \int_{\mathbb{S}^{d-1}} \frac{1}{N} \sum_{k=0}^{N-1} \mathbf{1}_{C(\tilde{\rho}\mathbf{x}_c + \sqrt{1-\tilde{\rho}^2}\mathbf{z}^*, \hat{\rho})}(\mathbf{x}_k) d\sigma_{d-1}(\mathbf{z}^*) \\ &= 2\hat{p}_1(\hat{\rho}) \mathbb{E}(p(\mathbf{y}, \hat{\rho})) \end{aligned}$$

for \mathbf{y} under Model 2. \square

Proof of Theorem 8

Proof. The proof follows from using Lemmas 7 to 10 and Theorem 7. \square